J. Fluid Mech. (2001), *vol.* 427, *pp.* 299–328. Printed in the United Kingdom

A unified approach for symmetries in plane parallel turbulent shear flows

By MARTIN OBERLACK†

Center for Turbulence Research, Stanford University, CA 94305-3030, USA

(Received 7 January 1997 and in revised form 31 July 2000)

A new theoretical approach for turbulent flows based on Lie-group analysis is presented. It unifies a large set of 'solutions' for the mean velocity of stationary parallel turbulent shear flows. These results are not solutions in the classical sense but instead are defined by the maximum number of possible symmetries, only restricted by the flow geometry and other external constraints. The approach is derived from the Reynolds-averaged Navier–Stokes equations, the fluctuation equations, and the velocity product equations, which are the dyad product of the velocity fluctuations with the equations for the velocity fluctuations. The results include the logarithmic law of the wall, an algebraic law, the viscous sublayer, the linear region in the centre of a Couette flow and in the centre of a rotating channel flow, and a new exponential mean velocity profile not previously reported that is found in the mid-wake region of high Reynolds number flat-plate boundary layers. The algebraic scaling law is confirmed in both the centre and the near-wall regions in both experimental and DNS data of turbulent channel flows. In the case of the logarithmic law of the wall, the scaling with the distance from the wall arises as a result of the analysis and has not been assumed in the derivation. All solutions are consistent with the similarity of the velocity product equations to arbitrary order. A method to derive the mean velocity profiles directly from the two-point correlation equations is shown.

1. Introduction

Under certain boundary and initial conditions, turbulent flows exhibit self-similar behaviour; some examples are jets, wakes, free and bounded shear flows. Von Kármán's law of the wall and Kolmogorov's inertial subrange also may be considered self-similar solutions in a certain flow regime. These findings lead to the hypothesis that turbulent flows locally tend to a self-similar state, provided the boundary and initial conditions are consistent. We obtain new solutions, which have not previously been found by dimensional analysis.

The logarithmic law was first derived by von Kármán (1930) using empirical models and dimensional arguments. Later Millikan (1939) derived the law of the wall more formally using the so called 'velocity defect law', which was also introduced by von Kármán (1930). Even though Millikan's derivation was much more comprehensive from a mathematical point of view, the velocity defect law has to be revised according to the present approach. This will be explained in detail in § 4.1. Yajnik (1970) and later Mellor (1972), extending Yajnik's work, derived the law of the wall using asymptotic methods solely based on the Navier–Stokes equations. Asymptotic forms

† Permanent address: Institut für Wasserbau und Wasserwirtschaft, Fachgebiet Hydromechanik und Hydraulik, TU Darmstadt, Petersenstraße 13, 64287 Darmstadt, Germany.

of the law of the wall, the velocity defect law, and the law of the wake have been obtained. However, no analytic functional form was found for the velocity defect law or the law of the wake.

Recently, some doubts have been expressed as to whether the appropriate wall-layer form is logarithmic or algebraic. Barenblatt (1993) developed an algebraic scaling law based on the idea of incomplete similarity with respect to the local Reynolds number. The proposed scaling law involves a special Reynolds number dependence of the power exponent and the multiplicative factor. The familiar logarithmic law is shown to be closely related to the envelope of a family of curves obeying power laws. George, Castillo & Knecht (1993) used an asymptotic invariance principle for zero-pressure-gradient turbulent boundary layer flows to suggest that the profiles in an overlap region between the inner and outer regions are power laws. In the limit of infinite Reynolds number, the usual logarithmic law of the wall was recovered in the inner region.

In the present approach a variety of scaling laws including the logarithmic and the algebraic law will be derived employing ideas from Lie group analysis. In a series of papers Ünal and Ibragimov (Ünal 1994, 1995; Ibragimov & Ünal 1994) have applied Lie group methods to Kolmogorov's inertial-subrange hypothesis. In the methodology of group theory the dissipation rate, as it was introduced by Kolmogorov, can be viewed as an invariant. Considering this, Ünal and Ibragimov investigated the symmetry properties of the Navier–Stokes equations and proposed a combined scaling group by imposing the dissipation rate invariance. As a result, they have shown that there are solutions of the Navier–Stokes equations which are consistent with Kolmogorov's proposal. However, the presented result is only a necessary and not a sufficient condition since it was not shown that the dissipation rate is always an invariant of turbulent flows if the Reynolds number tends to infinity.

In this paper, it will be shown by applying Lie group ideas to the Navier–Stokes equations that the von Kármán law of the wall is by no means the only non-trivial self-similar mean velocity profile which may be given explicitly. The set of mean velocity profiles obtained includes an algebraic law in the centre of a channel flow and in the near wall region, the viscous sublayer, the linear mean velocity in the centre of a Couette flow, the linear mean velocity in the centre of a rotating channel flow, and an exponential mean velocity profile. The exponential law in particular has not previously been reported in the literature. Here it is shown that such a law describes the outer part of a boundary layer flow over a flat plate and is in fact an explicit form of the velocity defect law. The word 'solution' used in the present context is somewhat different to its classical definition. For any of the turbulent flows mentioned above explicit mean velocity profiles are determined due to the maximum number of symmetries, only restricted by geometrical and other external constraints.

An introduction to the basic methodology of Lie's theory is given in the books by Bluman & Kumei (1989) and Stephani (1989).

The paper is organized as follows. In § 2 the governing equations are derived and the three major differences between the present approach and the classical approach using the Reynolds stress tensor equations (Townsend 1976) will be pointed out in detail. In § 3 the Lie group analysis and the somewhat different solution definition are described and the results for the self-similar mean flow profiles are given. In § 4 the new self-similar mean velocity profiles, also called scaling laws, are compared with experimental and direct numerical simulation (DNS) data. In the last section the results will be discussed and their applications to turbulence modelling are pointed out. Appendix A gives a proof that the self-similar profiles are also consistent with higher-

order velocity product equations. In Appendix B, all the self-similar mean velocities mentioned above have also been obtained by application of the Lie group analysis to the two-point correlation. Here also some new results regarding self-similarity of the two-point correlation tensor are obtained. In addition, a new non-parametric symmetry of the two-point correlation tensor in the log region is established.

2. Governing equations

Consider the incompressible Navier–Stokes equations in a constantly rotating frame,

$$\frac{\partial U_i}{\partial t} + U_k \frac{\partial U_i}{\partial x_k} = -\frac{\partial P}{\partial x_i} + \nu \frac{\partial^2 U_i}{\partial x_k \partial x_k} - 2\Omega_k \, e_{ikl} \, U_l \tag{2.1}$$

and the continuity equation

$$\frac{\partial U_k}{\partial x_k} = 0 \tag{2.2}$$

where U_i, P, ν and Ω_k are, respectively, the instantaneous velocity, pressure normalized by the density, kinematic viscosity and the angular rotation rate of the frame of reference relative to the inertial frame. Centrifugal forces have been absorbed into the pressure. Throughout the paper the Einstein summation convention has been employed.

The standard Reynolds decomposition is given by

$$U_i = \bar{u}_i + u_i \quad \text{and} \quad P = \bar{p} + p, \tag{2.3}$$

where the overbar denotes an ensemble average, defined as

$$\bar{u}_i = \lim_{n\to\infty} \frac{1}{n} \sum_{k=1}^{n} U_i^{(k)}, \quad \bar{p} = \lim_{n\to\infty} \frac{1}{n} \sum_{k=1}^{n} P_i^{(k)}. \tag{2.4}$$

From these the Reynolds-averaged Navier–Stokes equation follows

$$\frac{\partial \bar{u}_i}{\partial t} + \bar{u}_k \frac{\partial \bar{u}_i}{\partial x_k} = -\frac{\partial \bar{p}}{\partial x_i} + \nu \frac{\partial^2 \bar{u}_i}{\partial x_k^2} - \frac{\partial \overline{u_i u_k}}{\partial x_k} - 2\Omega_k \, e_{ikl} \, \bar{u}_l. \tag{2.5}$$

The fluctuation equations yield

$$\frac{\partial u_i}{\partial t} + \bar{u}_k \frac{\partial u_i}{\partial x_k} + u_k \frac{\partial \bar{u}_i}{\partial x_k} - \frac{\partial \overline{u_i u_k}}{\partial x_k} + \frac{\partial u_i u_k}{\partial x_k} + \frac{\partial p}{\partial x_i} - \nu \frac{\partial^2 u_i}{\partial x_k^2} + 2\,\Omega_k \, e_{ikl} \, u_l = 0. \tag{2.6}$$

The corresponding continuity equations for $\bar{u}_i$ and u_i are

$$\frac{\partial \bar{u}_k}{\partial x_k} = 0, \tag{2.7a}$$

$$\mathscr{C} = \frac{\partial u_k}{\partial x_k} = 0. \tag{2.7b}$$

In the case of a pressure-driven flow in the x_1-direction, the mean pressure $\bar{p}$ is replaced by $-x_1 K + \bar{p}(x_2)$, where K is a constant pressure gradient. The only axis of frame rotation to be considered is perpendicular to the mean shear, and hence $\Omega = \Omega_3$. The present analysis is restricted to stationary parallel shear flows

$$\frac{\partial \bar{u}_1}{\partial x_1} = \frac{\partial \bar{u}_1}{\partial x_3} = \frac{\partial \bar{u}_1}{\partial t} = \frac{\partial \bar{p}}{\partial x_1} = \frac{\partial \bar{p}}{\partial x_3} = \frac{\partial \bar{p}}{\partial t} = \bar{u}_2 = \bar{u}_3 = 0, \tag{2.8}$$

and hence $\bar{u}_1$ and $\bar{p}$ are only functions of the remaining spatial coordinate x_2. Thus, (2.5) reduces to

$$K + \nu \frac{\partial^2 \bar{u}_1}{\partial x_2^2} - \frac{\partial \overline{u_1 u_2}}{\partial x_2} = 0, \tag{2.9a}$$

$$-\frac{\partial \bar{p}}{\partial x_2} - \frac{\partial \overline{u_2 u_2}}{\partial x_2} - 2\,\Omega\,\bar{u}_1 = 0, \tag{2.9b}$$

$$\frac{\partial \overline{u_3 u_2}}{\partial x_2} = 0, \tag{2.9c}$$

and (2.6) becomes

$$\frac{\partial u_i}{\partial t} + \bar{u}_1 \frac{\partial u_i}{\partial x_1} + \delta_{i1} u_2 \frac{\mathrm{d}\bar{u}_1}{\mathrm{d}x_2} - \frac{\mathrm{d}\overline{u_i u_2}}{\mathrm{d}x_2} + \frac{\partial u_i u_k}{\partial x_k} + \frac{\partial p}{\partial x_i} - \nu \frac{\partial^2 u_i}{\partial x_k^2} + 2\,\Omega\, e_{i3l}\, u_l = 0. \tag{2.10}$$

The continuity equation (2.7*a*) for the mean velocity is trivially satisfied. It should be noted here that there is no restriction on the spatial or temporal dependence on the fluctuating quantities $\boldsymbol{u}$ and p.

The equations (2.9) are now rewritten and unified with the equation for the fluctuation (2.10) by solving (2.9*a*) and (2.9*b*) for the gradient of the Reynolds stresses and using the result in (2.10),

$$\begin{aligned}\mathscr{N}_i(\boldsymbol{x}) = {} & \frac{\partial u_i}{\partial t} + \bar{u}_1 \frac{\partial u_i}{\partial x_1} + \delta_{i1} u_2 \frac{\mathrm{d}\bar{u}_1}{\mathrm{d}x_2} - \delta_{i1} \left(K + \nu \frac{\partial^2 \bar{u}_1}{\partial x_2^2} \right) \\ & + \delta_{i2} \left(\frac{\partial \bar{p}}{\partial x_2} + 2\,\Omega\,\bar{u}_1 \right) + \frac{\partial u_i u_k}{\partial x_k} + \frac{\partial p}{\partial x_i} - \nu \frac{\partial^2 u_i}{\partial x_k^2} + 2\,\Omega\, e_{i3l}\, u_l = 0. \end{aligned} \tag{2.11}$$

The system of equations (2.11) describes the fluctuation and mean of a parallel turbulent shear flow. The set of equations is under-determined since the mean quantities are not known *a priori*. In the classical approach of finding turbulent scaling laws, this difficulty has motivated the introduction of second-moment equations (Townsend 1976). In the next section, the above set of equations (2.7*b*), (2.8) and (2.11) will be analysed with regard to its symmetry properties alone, without the introduction of higher-order correlation equations which contain more non-closed terms.

In order to do this, another equation is introduced which is derived from (2.11). It will be referred to as the 'instantaneous velocity product' equation

$$\mathscr{N}_i u_j + \mathscr{N}_j u_i = 0. \tag{2.12}$$

Usually, the Reynolds-averaged Navier–Stokes equation (2.5) and its simplification for plane shear flows (2.9*a–c*) have to be supplied with closure assumptions regarding the Reynolds stress tensor $\overline{u_i u_j}$. The common procedure to obtain transport equations for $\overline{u_i u_j}$ is Reynolds averaging (2.12). The purpose of (2.12) regarding the symmetry properties of plane shear flows is quite different as will be pointed out in § 3.1.

3. Lie point symmetries in turbulent parallel shear flows

Suppose the system of partial differential equations under investigation is given by

$$\boldsymbol{F}(\boldsymbol{y}, \boldsymbol{z}, \boldsymbol{z}^{(1)}, \boldsymbol{z}^{(2)}, \ldots) = 0, \tag{3.1}$$

where $\boldsymbol{y}$ and $\boldsymbol{z}$ are the independent and the dependent variables respectively and $\boldsymbol{z}^{(n)}$ refers to all nth-order derivatives of any component of $\boldsymbol{z}$ with respect to any component of $\boldsymbol{y}$. A transformation

$$\boldsymbol{y} = \boldsymbol{\phi}(\boldsymbol{y}^*, \boldsymbol{z}^*) \quad \text{and} \quad \boldsymbol{z} = \boldsymbol{\psi}(\boldsymbol{y}^*, \boldsymbol{z}^*) \tag{3.2}$$

is called a symmetry or symmetry transformation of equation (3.1) if the following equivalence holds:

$$\boldsymbol{F}(\boldsymbol{y}, \boldsymbol{z}, \boldsymbol{z}^{(1)}, \boldsymbol{z}^{(2)}, \ldots) = 0 \quad \Longleftrightarrow \quad \boldsymbol{F}(\boldsymbol{y}^*, \boldsymbol{z}^*, \boldsymbol{z}^{*(1)}, \boldsymbol{z}^{*(2)}, \ldots) = 0, \tag{3.3}$$

i.e. the transformation (3.2) substituted into (3.1) does not change the form of equation (3.1) if written in the new variables $\boldsymbol{y}^*$ and $\boldsymbol{z}^*$.

In the present approach the classical group analysis is modified towards an equivalence transformation. It is assumed that the equations under investigation are transformed to equations of the same family. This means that given a set of differential equations containing one or several free functions the equivalence transformation does not change the structure of the differential equation. However the free functions may be altered in form. Hence the differential equation is not transformed to an identical equation in a strict sense but to one which is identical in form apart from the free functions.

In the present context the quantities ν, $\bar{p}$ and particularly the mean velocity $\bar{u}_1$ may exhibit different forms in the equations (2.7*b*)–(2.12) under the transformation. Hence, subsequently, different submodels or subclasses will be considered especially those depending on the functional form of $\bar{u}_1$. We focus specifically on those mean velocities which allow a large number of symmetries in the equations (2.7*b*)–(2.12). The latter is essentially the 'maximum symmetry principle' determining $\bar{u}_1$, which will be explained in some more detail below.

Though in principle only simple algebraic calculations need to be performed the above concepts applied to systems of partial differential equations can be extremely tedious and lengthy if the number of equations is larger than two or the equations contain derivatives of order higher than two. Lie's procedure to find symmetry transformations and the derivation of self-similar solutions may be divided into three parts. The first one, the computation of the determining system, is completely algorithmic. Several Lie group software packages for the computation of the determining system have been developed. All the presented results have been obtained with the aid of SYMMGRP.MAX, a software package for MACSYMA (1996) written by Champagne, Hereman & Winternitz (1991). The second part, the solution of the determining system, which is a linear over-determined system of partial differential equations, must be done by hand. The last part, the computation of the similarity variables, involves the solution of first-order differential equations which are usually easy to solve.

The set of variables considered in the calculation below consists of

$$\boldsymbol{y} = [x_1,\ x_2,\ x_3,\ t,\ \nu] \quad \text{and} \quad \boldsymbol{z} = [u_1,\ u_2,\ u_3,\ p,\ \bar{u}_1,\ \bar{p}], \tag{3.4}$$

where $\boldsymbol{y}$ and $\boldsymbol{z}$ represent the independent and dependent variables respectively. The usual purpose of the symmetry analysis is to find all those invertible transformations,

$$\left.\begin{aligned} \boldsymbol{y}^* &= [x_1^*,\ x_2^*,\ x_3^*,\ t^*,\ \nu^*] = \boldsymbol{\phi}(\boldsymbol{y}, \boldsymbol{z}; \varepsilon), \\ \boldsymbol{z}^* &= [u_1^*,\ u_2^*,\ u_3^*,\ p^*,\ \bar{u}_1^*,\ \bar{p}^*] = \boldsymbol{\psi}(\boldsymbol{y}, \boldsymbol{z}; \varepsilon), \end{aligned}\right\} \tag{3.5}$$

which, in the consideration of (2.8), preserve the functional form of (2.7*b*), (2.11), and

(2.12) written in the new variables $\boldsymbol{y}^*$ and $\boldsymbol{z}^*$. In other words, a transformation of the form (3.5) will be computed so that the following equivalence holds:

$$\mathscr{C} = 0 \quad \Longleftrightarrow \quad \mathscr{C}^* = 0, \tag{3.6a}$$

$$\mathscr{N}_i = 0 \quad \Longleftrightarrow \quad \mathscr{N}_i^* = 0, \tag{3.6b}$$

$$(\mathscr{N}_i u_j + \mathscr{N}_j u_i) = 0 \quad \Longleftrightarrow \quad (\mathscr{N}_i u_j + \mathscr{N}_j u_i)^* = 0. \tag{3.6c}$$

The superscript * of any quantity denotes its evaluation according to the transformation (3.5). The transformations $\boldsymbol{\phi}$ and $\boldsymbol{\psi}$ are invertible mappings which depend on the group parameter ε. Here, viscosity will also be introduced as an additional independent variable. Allowing a parameter such as ν to vary is also part of the equivalence transformation. In the present context this is justified since viscosity may be considered the inverse of the Reynolds number because $\nu \sim 1/Re$. In most practical applications the Reynolds number can be varied arbitrarily. The idea of varying ν may have been first applied to Navier–Stokes equations in their classical form by Ünal (1994). In the present investigation the equivalence transformation allows a Reynolds number dependence of the scaling law coefficients. However, beside this modification all the scaling laws originate purely from the inviscid forces in the Navier–Stokes equations as can also be taken from the inviscid two-point approach in Appendix B.

It should be noted that a transformation of the form (3.4) does not imply any dependence among variables. It only refers to a transformation to a new set of variables here denoted by an asterisk. In particular it does not indicate any spatial or time dependence of the molecular viscosity.

Lie has shown that if a transformation has group properties it can be represented by its infinitesimal form. For the transformation (3.5) this means that it can be be expanded for small ε:

$$\left.\begin{aligned} \boldsymbol{y}^* &= \boldsymbol{y} + \varepsilon \left.\frac{\partial \boldsymbol{\phi}}{\partial \varepsilon}\right|_{\varepsilon=0} + O(\varepsilon^2) = \boldsymbol{y} + \varepsilon\, \boldsymbol{\xi}(\boldsymbol{y},\boldsymbol{z}) + O(\varepsilon^2), \\ \boldsymbol{z}^* &= \boldsymbol{z} + \varepsilon \left.\frac{\partial \boldsymbol{\psi}}{\partial \varepsilon}\right|_{\varepsilon=0} + O(\varepsilon^2) = \boldsymbol{z} + \varepsilon\, \boldsymbol{\eta}(\boldsymbol{y},\boldsymbol{z}) + O(\varepsilon^2). \end{aligned}\right\} \tag{3.7}$$

From this expansion only the terms of order ε need to be considered since the global form of the transformation can be recovered by employing Lie's differential equation

$$\frac{\mathrm{d}\boldsymbol{y}^*}{\mathrm{d}\varepsilon} = \boldsymbol{\xi}(\boldsymbol{y}^*,\boldsymbol{z}^*) \quad \text{and} \quad \frac{\mathrm{d}\boldsymbol{z}^*}{\mathrm{d}\varepsilon} = \boldsymbol{\eta}(\boldsymbol{y}^*,\boldsymbol{z}^*) \tag{3.8}$$

subject to the initial conditions

$$\boldsymbol{y}^*(\varepsilon = 0) = \boldsymbol{y} \quad \text{and} \quad \boldsymbol{z}^*(\varepsilon = 0) = \boldsymbol{z}. \tag{3.9}$$

The terms $\boldsymbol{\xi}$ and $\boldsymbol{\eta}$ are called infinitesimals.

Omitting all the higher-order terms, the elements of $\boldsymbol{y}^*$ and $\boldsymbol{z}^*$ in (3.7) may be rewritten as

$$\left.\begin{aligned} &x_1^* = x_1 + \varepsilon\xi_{x_1},\ x_2^* = x_2 + \varepsilon\xi_{x_2},\ x_3^* = x_3 + \varepsilon\xi_{x_3},\ t^* = t + \varepsilon\xi_t,\ v^* = v + \varepsilon\xi_v, \\ &u_1^* = u_1 + \varepsilon\eta_{u_1},\ u_2^* = u_2 + \varepsilon\eta_{u_2},\ u_3^* = u_3 + \varepsilon\eta_{u_3}, \\ &p^* = p + \varepsilon\eta_p,\ \bar{u}_1^* = \bar{u}_1 + \varepsilon\eta_{\bar{u}_1},\ \bar{p}^* = \bar{p} + \varepsilon\eta_{\bar{p}}, \end{aligned}\right\} \tag{3.10}$$

where, instead of the mapping $\boldsymbol{\phi}$ and $\boldsymbol{\psi}$, only the infinitesimal generators $\boldsymbol{\xi}$ and $\boldsymbol{\eta}$ need to be determined. The subscripts of the elements of $\boldsymbol{\xi}$ and $\boldsymbol{\eta}$ indicate the variables they

refer to and are not to be mistaken as derivatives. Given the infinitesimal generators $\boldsymbol{\xi}$ and $\boldsymbol{\eta}$, the global transformations $\boldsymbol{\phi}$ and $\boldsymbol{\psi}$ are uniquely determined by (3.8) and (3.9). The major advantage of the infinitesimal approach is that the equations for the infinitesimal generators are linear and, generally, easy to solve.

Practically speaking, it is impossible to determine $\boldsymbol{\phi}$ and $\boldsymbol{\psi}$ from (3.6*a–c*) using the global transformation (3.5) directly, as this results in a large, over-determined system of non-linear PDEs for $\boldsymbol{\phi}$ and $\boldsymbol{\psi}$ which is intractable to solve.

In order to obtain the infinitesimals $\boldsymbol{\xi}$ and $\boldsymbol{\eta}$, (3.10) is inserted into the equations (3.6*a–c*) and expanded with respect to ε. For example, introducing (3.10) into the equation on the right-hand side of (3.6*a*) reduces it to $\mathscr{C}^* = \mathscr{C} + \varepsilon \mathrm{X}\mathscr{C} + O(\varepsilon^2)$. Making use of the equation on the left-hand side of (3.6*a*), the leading-order equation reduces to $\mathrm{X}\mathscr{C} = 0$, where use has already been made of the fact that only terms of order ε need to be considered. Here, X is the operator

$$\mathrm{X} = \xi_{x_1}\frac{\partial}{\partial x_1} + \xi_{x_2}\frac{\partial}{\partial x_2} + \xi_{x_3}\frac{\partial}{\partial x_3} + \xi_t\frac{\partial}{\partial t} + \xi_v\frac{\partial}{\partial v}$$

$$+\eta_{u_1}\frac{\partial}{\partial u_1} + \eta_{u_2}\frac{\partial}{\partial u_2} + \eta_{u_3}\frac{\partial}{\partial u_3} + \eta_p\frac{\partial}{\partial p} + \eta_{\bar{u}_1}\frac{\partial}{\partial \bar{u}_1} + \eta_{\bar{p}}\frac{\partial}{\partial \bar{p}} + \mathrm{X}_p \tag{3.11}$$

and X_p is referred to as the 'prolongation' up to the second order. The prolongation appears due to the infinitesimal transformation of the derivatives and it leads to derivatives of the generators $\boldsymbol{\xi}$ and $\boldsymbol{\eta}$. This may be verified by calculating the derivatives of the dependent variable with respect to the independent variables using the infinitesimal transformation (3.10). Expanding in ε and keeping only terms to order ε the form of the prolongation may be obtained.

Extending the procedure described above for the continuity equation to the other equations under investigation namely (2.7*b*), (2.11), and (2.12), their symmetries can be determined by applying the operator (3.11) to them. This results in the set of equations

$$\mathrm{X}\mathscr{C}|_{\mathscr{C}=0} = 0, \tag{3.12a}$$

$$\mathrm{X}\mathscr{N}_i|_{\mathscr{N}_i=0} = 0, \tag{3.12b}$$

$$\mathrm{X}(\mathscr{N}_i u_j + \mathscr{N}_j u_i)|_{(\mathscr{N}_i u_j + \mathscr{N}_j u_i)=0} = 0, \tag{3.12c}$$

which has to be furnished by the geometrical restrictions (2.8). The equations (3.12*a–c*) may be considered as a set of equations for $\boldsymbol{\xi}$ and $\boldsymbol{\eta}$, containing all variables $\boldsymbol{y}$ and $\boldsymbol{z}$ including all derivatives of only u_1, u_2, u_3, p, $\bar{u}_1$, $\bar{p}$ with respect to all independent variables x_1, x_2, x_3, t, v, up the second order. Each of the variables in $\boldsymbol{y}$ and $\boldsymbol{z}$ and its derivatives needs to be considered an independent variable. Since the equations (3.12*a–c*) have to be solved for all values of the latter variables, a large over-determined system of linear equations for $\boldsymbol{\xi}$ and $\boldsymbol{\eta}$ has to be solved. The solution will be given in the following two subsections.

The present approach of equivalence transformations takes into account that the system (2.7*b*), (2.11), and (2.12) comprises variables which exhibit chaotic and non-chaotic character. By definition the mean quantities $\bar{\boldsymbol{u}}$ and $\bar{p}$ are 'smooth' functions of space and time. In contrast, the fluctuating quantities $\boldsymbol{u}$ and p exhibit chaotic behaviour.

This procedure implies two immediate consequences leading to the definition of the 'maximum symmetry principle' to be pointed out below. First, the equivalence

transformation technique does not indicate a similarity solution for both the mean and the fluctuating quantities as it is the usual result employing classical Lie group analysis. Instead, the fluctuating quantities may still exhibit a chaotic behaviour.

Second, and most important, the mean velocities obtained by this method are not a solution of any equation in the classical sense. They are merely a consequence of the assumption that the mean velocity adjusts itself such that the maximum number of combined symmetries is established. This is to be defined in the following.

The fact that certain chaotic spatio-temporal systems admit a wider degree of symmetries is well documented for several systems (see e.g. Dellnitz, Golubitsky & Melbourne 1992; Field & Golubitsky 1995; Ning *et al.* 1993). These additional symmetries appear beyond a certain threshold of a bifurcating parameter which may in the present context be identified as the Reynolds number.

In fact, Kolmogorov's inertial-subrange theory of locally isotropic turbulence may be regarded as an example of the above finding. The theory of isotropic turbulence comprises invariance under the full rotation group, translation in space and time and Galilean invariance. Hence, isotropic turbulence admits invariance under a very large number of symmetry groups.

In contrast such a high degree of invariance under many distinct groups cannot be expected for large-scale quantities and a much less restrictive definition of a 'maximum symmetry principle' may be introduced in the present context.

Symmetry groups of differential equations span a linear vector space and hence can be linearly combined. Strictly speaking a given linear combination of symmetries constitutes only a single symmetry. Hence, in the following we define the 'maximum symmetry principle' by assuming that the mean flow quantities establish themselves such that a maximum of linearly combined symmetries is the basis for the flow profiles. These symmetries are only restricted by boundary conditions and other external constraints. For simplicity we frequently denote these mean velocities as solutions.

Though it is known that the mean quantities have a strong tendency towards a high degree of symmetry and similarity this is usually only observed in simple flow geometries. It is still an outstanding question why this type of mean velocity profiles appears to be strong attractor of statistical turbulence. Furthermore, even if we do assume that these mean profiles exist it is not obvious *a priori* to which real flow region of plane shear flows the different functional forms for $\bar{u}_1$ can be assigned. DNS and experimental data need to be employed as shown in the next subsection. However, it is important to note that group theoretical arguments very much guide the finding of these flow regions where the 'high symmetric' mean velocity profiles are applicable.

For the present purpose of finding mean velocities comprising a high degree of symmetry the equations

$$\frac{\mathrm{d}v}{\xi_v} = \frac{\mathrm{d}x_2}{\xi_{x_2}} = \frac{\mathrm{d}\bar{u}_1}{\eta_{\bar{u}_1}} \tag{3.13}$$

need to be considered since $\bar{u}_1$ only depends on x_2 and v. Any other dependence is excluded due to the geometrical constraints (2.8).

3.1. *Determining the infinitesimals and the symmetry breaking property of* (2.12)

Recall that, in the first step of the present approach the infinitesimal generators must be determined from the equations (3.12*a*, *b*). This is accomplished using SYMM-GRP.MAX, a package for MACSYMA (1996) written by Champagne *et al.* (1991). As a result, an over-determined set of more than one hundred linear PDEs (not

shown here) is obtained, whose solution is

$$\left.\begin{aligned}
\xi_{x_1} &= a_1(v)x_1 + a_2(v)x_3 + f_1(t,v),\\
\xi_{x_2} &= a_1(v)x_2 + a_3(v),\\
\xi_{x_3} &= a_1(v)x_3 - a_2(v)x_1 + f_2(t,v),\\
\xi_t &= a_4(v)t + a_5(v),\\
\xi_v &= [2a_1(v) - a_4(v)]v,\\
\eta_{u_1} &= [a_1(v) - a_4(v)]u_1 + a_2(v)u_3 + \frac{\mathrm{d}f_1}{\mathrm{d}t} - g_1(x_2,\bar{u}_1,\bar{p},v),\\
\eta_{u_2} &= [a_1(v) - a_4(v)]u_2,\\
\eta_{u_3} &= [a_1(v) - a_4(v)]u_3 - a_2(v)[u_1 + \bar{u}_1] + \frac{\mathrm{d}f_2}{\mathrm{d}t}\\
\eta_p &= 2[a_1(v) - a_4(v)]p - x_1\left[\frac{\mathrm{d}^2 f_1}{\mathrm{d}t^2} + [a_1(v) - 2a_4(v)]K\right]\\
&\quad -x_3\left[\frac{\mathrm{d}^2 f_2}{\mathrm{d}t^2} - a_2(v)K\right] - g_2(x_2,\bar{u}_1,\bar{p},v) + f_3(t,v),\\
\eta_{\bar{u}_1} &= [a_1(v) - a_4(v)]\bar{u}_1 + g_1(x_2,\bar{u}_1,\bar{p},v),\\
\eta_{\bar{p}} &= 2[a_1(v) - a_4(v)]\bar{p} + g_2(x_2,\bar{u}_1,\bar{p},v).
\end{aligned}\right\} \tag{3.14}$$

Note that all of the undetermined functions in (3.14) depend upon viscosity. In particular it should be remarked that the infinitesimal generator for v does not have any dependence on variables other than viscosity itself. Using this in conjunction with Lie's differential equation (3.8), from which the global transformation can be obtained, it can be concluded that only symmetry transformation of the form $v^* = f(v)$ exist.

Later, for the derivation of the mean velocity profiles, it will be argued that, for the flows to be focused on, the large Reynolds number limit is applicable and to leading order any v dependence will be neglected.

The generators (3.14) contain five undetermined functions: f_1, f_2, and f_3 which depend on t, and g_1 and g_2 which depend on x_2, $\bar{u}_1$, and $\bar{p}$. The appearance of g_1 and g_2 in the generators is due to the fact that the system consisting of (2.7) and (2.11) is under-determined.

In particular, g_1 allows for any arbitrary mean velocity $\bar{u}_1$ in the equation (3.13). Of course, this strongly contradicts experiments since the mean profiles always converge to some kind of universal profile. Hence the additional constraint (2.12) is introduced to determine the functional form of g_1. This restriction is symmetry breaking in order to find a definite form for the functions g_1.

It has been pointed out at the end of § 2 that (2.12) is crucial to find self-similar mean velocity profiles consistent with the second moment and all higher-order correlation equations. Hence, the extended set of equations consisting of (3.12*a–c*) is considered to compute the infinitesimals.

After the infinitesimals (3.14) have been determined from (3.12*a*, *b*) they may in a second step be subjected to the additional restriction (3.12*c*). Carrying out the differentiations in (3.12*c*) we find

$$\mathscr{N}_i \,\mathrm{X}u_j + \mathscr{N}_j \,\mathrm{X}u_i + u_j \,\mathrm{X}\mathscr{N}_i + u_i \,\mathrm{X}\mathscr{N}_j = 0. \tag{3.15}$$

The last two terms do not contribute to the constraints for the infinitesimals since $\mathscr{N}_i u_j + \mathscr{N}_j u_i$ may be factored out. Due to (2.12) this term cancels. After applying the operator X given by (3.11) the remaining first two terms in (3.15) become

$$\mathscr{N}_i \eta_{u_j} + \mathscr{N}_j \eta_{u_i} = 0. \tag{3.16}$$

The term $\mathscr{N}_i u_j + \mathscr{N}_j u_i$ may again be separated out from (3.15). Since this term also cancels out due to (2.12) we obtain the remaining restrictions

$$\left.\begin{aligned} a_2(v)u_3 + \frac{\mathrm{d}f_1}{\mathrm{d}t} - g_1(x_2, \bar{u}_1, \bar{p}, v) = 0, \\ -a_2(v)[u_1 + \bar{u}_1] + \frac{\mathrm{d}f_2}{\mathrm{d}t} = 0, \end{aligned}\right\} \tag{3.17}$$

coming particularly from the infinitesimals η_{u_1} and η_{u_3}. Since (3.17) has to be true for arbitrary values of its arguments we find the general solution

$$\left.\begin{aligned} a_2(v) &= 0, \\ f_2(t, v) &= b_3(v), \\ g_1(x_2, \bar{u}_1, \bar{p}, v) &= b_1(v), \\ f_1(t, v) &= b_1(v)t + b_2(v). \end{aligned}\right\} \tag{3.18}$$

This additional set of equations is symmetry breaking. The resulting reduced set of final generators is given by

$$\left.\begin{aligned} \xi_{x_1} &= a_1(v)x_1 + b_1(v)t + b_2(v), \\ \xi_{x_2} &= a_1(v)x_2 + a_3(v), \\ \xi_{x_3} &= a_1(v)x_3 + b_3(v), \\ \xi_t &= a_4(v)t + a_5(v), \\ \xi_v &= [2a_1(v) - a_4(v)]v, \\ \eta_{u_1} &= [a_1(v) - a_4(v)]u_1, \\ \eta_{u_2} &= [a_1(v) - a_4(v)]u_2, \\ \eta_{u_3} &= [a_1(v) - a_4(v)]u_3, \\ \eta_p &= 2[a_1(v) - a_4(v)]p + g_2(x_2, \bar{u}_1, \bar{p}, v) - x_1[a_1(v) - 2a_4(v)]K + f_3(t, v), \\ \eta_{\bar{u}_1} &= [a_1(v) - a_4(v)]\bar{u}_1 + b_1(v), \\ \eta_{\bar{p}} &= 2[a_1(v) - a_4(v)]\bar{p} - g_2(x_2, \bar{u}_1, \bar{p}, v). \end{aligned}\right\} \tag{3.19}$$

Using (3.13), the mean velocities may be computed, since g_1 in (3.14) has been reduced to $b_1(v)$ in (3.19).

The infinitesimal generators (3.19) comprise all symmetries admitted by the equation for the continuity (2.7), the equation for the velocity fluctuation (2.11) and the second-order velocity product equation (2.12). It should be noted that $b_1(v)$ corresponds to the Galilean group in infinitesimal form. Apparently, the fluctuating quantities are not affected by the Galilean group since none of the η_{u_i} contain $b_1(v)$.

The consequences of (2.12) for the Galilean invariance of the mean and the

fluctuating quantities may be more clearly understood on the basis of the global variables. The Galilean transformation group of the instantaneous variables in its general form is given by

$$t^* = t, \quad x_i^* = x_i + a_i t, \quad U_i^* = U_i + a_i, \quad P^* = P, \tag{3.20}$$

where a_i is an arbitrary constant vector of dimension velocity.

Employing the Reynolds decomposition (2.3) it is not obvious *a priori* whether the arbitrary velocity a_i 'transfers' to the mean or the fluctuating velocity or may even split into different parts.

In the following it will be shown that the arbitrary velocity a_i in (3.20) 'moves' to the mean velocity. The most simple method of proving this is given by applying the ensemble average operator (2.4) to (3.20). As a result we obtain

$$t^* = t, \quad x_i^* = x_i + a_i t, \quad \bar{u}_i^* = \bar{u}_i + a_i, \quad \bar{p}^* = \bar{p}, \tag{3.21}$$

while from (2.3) it immediately follows that

$$u_i^* = u_i \quad \text{and} \quad p^* = p. \tag{3.22}$$

This invariant transformation can be verified by introducing (3.21) and (3.22) into (2.5) and (2.7*a*). In fact, any other partition of a_i between $\bar{u}_i$ and u_i other than those in (3.21) and (3.22) leads to a contradiction.

In the present case only plane steady shear flows are considered which leads to the very restricted form of momentum equations (2.9*a–c*). Apart from near-wall regions where viscosity plays a dominant role, the equations (2.9*a–c*) do not provide any information on the mean velocity. Instead only certain Reynolds stresses can be determined. In classical semi-empirical turbulence modelling approaches model equations for the stresses have to be used which determine the mean velocity.

It is the paradox of plane shear flows that the mean velocity is determined by the stresses while parts of the stresses are determined by the mean momentum equations. This problem has to be accounted for also in the present context of finding mean velocity profiles using symmetry methods.

The major difference between the classical turbulence modelling approach and the present procedure is the treatment of equation (2.12). For the current treatment averaging is not necessary and indeed not useful since additional unknown terms would enter the set of equations. Instead (2.12) provides the necessary information regarding the Galilean invariance. Since the mean momentum equations (2.9*a–c*) do not give any information regarding the splitting of a_i among $\bar{u}_i$ and u_i this knowledge is supplied by (2.12). It is obvious that (2.12) is only form-invariant under the Galilean transformation group if the transformations (3.21) and (3.22) are employed.

In Appendix A it is shown that any scaling law for the velocity fluctuation and the second-order velocity product equations (2.12) is also a scaling law for all nth-order velocity product equations. The nth-order velocity product equations are defined as the nth-order dyadic product of the velocity fluctuations with the equation for the velocity fluctuations. Since the averaging procedure does not change the scaling properties of the nth-order velocity product equations, it is also consistent with all nth-order correlation equations. In the classical approach using correlation functions, it may be difficult to show that all higher-order velocity correlations are consistent with the scaling in the Reynolds stress equations. The Reynolds stress equations are the first of an infinite sequence of correlation equations which need to be considered in the classical approach in order to achieve the same level of consistency.

3.2. *Similarity and large Reynolds number limit*

Up to this point dependence on viscosity or Reynolds number has not been discussed. As shown by (3.19) all group parameters may depend on viscosity or Reynolds number. As a result, which can also be taken from the infinitesimals in (3.19), the functional form of the Reynolds number dependence may not be determined explicitly.

Nevertheless, turbulent flows exhibit the well-known feature of Reynolds number independence as Reynolds number tends to infinity. This has been observed in a large number of experiments (see e.g. Cantwell 1981). For the present purpose this fact may be translated to an assumption for certain functions depending on ν. Namely, it will be postulated that any function depending on ν is 'well behaved' in the sense that it is not vanishing and not diverging as ν tends to zero.

In fact, this assumption is fully equivalent to an approach where viscosity had been neglected right from the beginning and only the Euler equations had been considered. The reason is the following. Investigating the Euler equations instead of the Navier–Stokes equations leads to identical infinitesimals (3.14) and (3.19) with one exception. There would be no ν dependence in any of the free functions such as a_i or b_i. Hence a_i or b_i would be essentially constants. From this perspective we may conclude that if the degenerate cases of a_i or b_i being zero are excluded all scaling laws to be obtained in the following are dominated by the Euler terms or in other words by the inertial forces.

To this effect, the above small viscosity assumption is applied to the group parameters where it is assumed that

$$\lim_{\nu\to 0} k(\nu) = \text{finite}; \tag{3.23}$$

$k(\nu)$ is a representative of any group parameter in (3.19). Hence, in the limit of small viscosity or large Reynolds numbers, the leading-order form of $\bar{u}_1$ and $\bar{p}$ may be assumed to be independent of viscosity. Note that this assumption does not restrict the number or the functional form of the self-similar flow profiles to be computed later. It simply restricts the constants appearing in the self-similar mean velocity profiles to be independent of viscosity. An explicit Reynolds number dependence of the scaling laws will be investigated in the future, as this functional dependence may not be captured with the present analysis.

The equation (3.13) and the generators for x_2, ν and $\bar{u}_1$ in (3.19) can be combined into

$$\frac{\mathrm{d}\nu}{[2a_1 - a_4]\nu} = \frac{\mathrm{d}x_2}{a_1 x_2 + a_3} = \frac{\mathrm{d}\bar{u}_1}{[a_1 - a_4]\bar{u}_1 + b_1} \tag{3.24}$$

where the simplification (3.23) has already been implied. The last two equations constitute the condition for $\bar{u}_1$ comprising a maximum degree of symmetries.

In order to obtain mean velocity profiles from (3.24) the usual procedure is to first integrate the set of equations for the independent variables. Here, this is the equation on the left-hand side which for arbitrary and non-zero a_1–a_4 leads to $\zeta = \nu/(x_2 + a_3/a_1)^{2-a_4/a_1}$ where ζ is a constant of integration. In a second step the equation on the right-hand side is integrated to $\bar{u}_1 = \sigma(x_2 + a_3/a_1)^{1-a_4/a_1} - b_1/(a_1 - a_4)$ where σ is a constant of integration. Usually, ζ and σ are taken as the new independent and dependent variables respectively where σ may depend on ζ.

For the present purpose of investigating similarity mean velocity profiles in the large Reynolds number limit one may follow (3.23) by presuming an equivalent assumption for the dependence $\sigma(\zeta)$. Since ζ depends directly on ν it is taken that

$$\lim_{\nu\to 0} \sigma(\zeta) = \text{finite}. \tag{3.25}$$

Integrating the equation (3.24) by inferring (3.23) and (3.25) results in several fundamentally different self-similar flow profiles for certain combinations of the parameters contained in them.

Each of the group parameters in (3.24) or rather (3.19) has a distinct physical meaning; a_1 and a_4 correspond to a scaling group. This corresponds to the fact that all variables and parameters of the equation under consideration can be scaled by an arbitrary factor without changing the structure of the equation. Since their role in the solutions is particularly important a detailed discussion is given below. The group parameter b_1 conforms to the classical Galilean group. The Galilean boost has its counterpart in the transformation of the x_1-coordinate which, given in infinitesimal form, corresponds to the second term on the right-hand side of the equation for ξ_{x_1} in (3.19). The parameter a_3 corresponds to the translation group in the x_2-direction. The change of the origin of the coordinate x_2 by the arbitrary parameter a_3 does not alter the equation under investigation.

The remaining parameters b_2, b_3, a_5, g_2 and f_3 do not appear in the equation for the mean velocity but illuminate important physical properties of the plane shear flow case. Parameters b_2 and b_3 have a similar meaning as a_3, i.e. the origin of the spatial coordinates x_1 and x_3 can be altered without changing the underlying equations. The function g_2 still depends on x_2, $\bar{u}_1$ and $\bar{p}$ in an unknown form. Since g_2 appears in the transformation of both the mean and fluctuating pressure the functional dependence of the mean pressure cannot be determined. Beside its dependence on ν the function f_3 also depends on time t. This is a consequence of the Navier–Stokes equations for an incompressible fluid. Therein the pressure only appears as a gradient. For this reason the background pressure can arbitrarily be varied with time.

It is in particular the physical interpretation of the scaling parameters a_1 and a_4 which is crucial in order to understand each scaling law to follow. For this reason we give the global transformations which belong to the parameters a_1 and a_4 by employing Lie's differential equations (3.8) and (3.9). As a result the global transformation is

$$\left.\begin{aligned} &\boldsymbol{x}_i^* = \mathrm{e}^{a_1}\boldsymbol{x}_i, \quad t^* = \mathrm{e}^{a_4}t, \quad \nu^* = \mathrm{e}^{2a_1-a_4}\nu, \quad \boldsymbol{u}_i^* = \mathrm{e}^{a_1-a_4}\boldsymbol{u}_i, \\ &p^* = \mathrm{e}^{2(a_1-a_4)}p, \quad \bar{u}_1^* = \mathrm{e}^{a_1-a_4}\bar{u}_1, \quad \bar{p}^* = \mathrm{e}^{2(a_1-a_4)}\bar{p}. \end{aligned}\right\} \tag{3.26}$$

Consider the parameter a_1: e^{a_1} appears as a factor of all spatial coordinates in (3.26). This means that all spatial coordinates can be scaled if the appropriate velocity scale is also introduced. Suppose a given external length scale l, as a boundary value say, is present in the flow under investigation. As a consequence, the scaling symmetry with respect to the spatial coordinates is lost since l is a fixed quantity. Consequently, a_1 can only be zero in (3.26). Subsequently, any of the parameters being zero is referred to as a 'broken symmetry'.

Each of the velocity profiles to be computed below and its associated symmetries may be interpreted in terms of a given external length, time or velocity scale breaking some of the scaling symmetries. Consider the case $a_4 = 0$: from (3.26) it is deduced that there is an external time scale acting on the flow and hence there is no scaling symmetry with respect to the time t. If $a_1 = a_4$ the scaling symmetry for the velocities is broken and as a consequence the time and length scales have the same scaling properties. Any coordinate, in the latter cases $\boldsymbol{x}$, t and $\boldsymbol{u}$, is referred to as an invariant if it does not admit a scaling symmetry. In the following, each of the self-similar flow profiles integrated from the equations (3.24) will be explained separately.

A non-zero angular rotation rate will be considered only in § 3.4. In this case, the

set of transformations to be obtained contains a reduced number of parameters. The rotation rate will be considered as a branching parameter for the two cases $\Omega = 0$ and $\Omega \neq 0$.

3.3. *Scaling of turbulent shear flows with zero system rotation*

3.3.1. *Algebraic mean velocity profile:* $a_1 \neq a_4 \neq 0$ *and* $b_1 \neq 0$

The present case is the most general. No scaling symmetry is broken. As a result, the mean velocity $\bar{u}_1$ has the form

$$\bar{u}_1 = C_1(x_2 + c_1)^{1-c_2} - \frac{c_3}{1-c_2}, \tag{3.27}$$

where

$$c_1 = \frac{a_3}{a_1}, \quad c_2 = \frac{a_4}{a_1}, \quad c_3 = \frac{b_1}{a_1}. \tag{3.28}$$

In the domain where the algebraic mean velocity profile is valid, there is no external length or velocity scale acting directly on the flow, as non-zero and unequal parameters a_1 and a_4 are needed for its derivation. It will be pointed out in §4 that the case of an algebraic scaling law applies both in the vicinity of the wall, as has been suggested by Barenblatt (1993) and George *et al.* (1993), as well as in the centre region of a channel flow.

3.3.2. *Logarithmic mean velocity profile:* $a_1 = a_4 \neq 0$ *and* $b_1 \neq 0$

For the present combination of parameters, the infinitesimals (3.19) demonstrate that no scaling symmetry with respect to the velocities exists and hence an external velocity scale is symmetry breaking. The mean velocity $\bar{u}_1$ may be integrated to a generalized form of the familiar log law

$$\bar{u}_1 = d_2 \log(x_2 + d_1) + C_2, \tag{3.29}$$

with

$$d_1 = \frac{a_3}{a_1}, \quad d_2 = \frac{b_1}{a_1}. \tag{3.30}$$

In the case of the classical logarithmic law of the wall, it is the friction velocity u_τ which breaks the scaling symmetry for the velocities. The present case coincides with the usual derivation of the logarithmic law of the wall where the friction velocity u_τ is the only velocity scale in the near-wall region. To date a logarithmic scaling law has only been found in the vicinity of a wall where in the classical form the constant d_1 is set to zero.

Since the scaling symmetry with respect to the spatial variables ($a_1 \neq 0$) is still retained the length scale varies linearly with the distance to the wall. This is an assumption in the classical derivation of the log law of the wall but is a result of the present analysis.

3.3.3. *Exponential mean velocity profile:* $a_1 = 0$ *and* $a_4 \neq b_1 \neq 0$

Since a_1 is zero in the present case, there exists an external length scale which breaks the symmetry with respect to the spatial coordinates. As a result $\boldsymbol{x}$ is an invariant with only a constant added to the infinitesimal in (3.19) resulting from the frame invariance.

The mean velocity $\bar{u}_1$ turns out to have the form

$$\bar{u}_1 = \frac{e_2}{e_1} + \exp(-e_1 x_2) C_3, \tag{3.31}$$

where

$$e_1 = \frac{a_4}{a_3}, \quad e_2 = \frac{b_1}{a_3}. \tag{3.32}$$

It will be shown in § 4 that the present case applies to the flat-plate high Reynolds number boundary layer flow. It appears that the boundary layer thickness is the external length scale which is symmetry breaking.

3.3.4. *Linear mean velocity profile:* $a_1 = a_4 = 0$ *and* $b_1 \neq a_3 \neq 0$

In the present case there is an external velocity and length scale present in the flow and all variables $\boldsymbol{u}$, p, $\boldsymbol{x}$ and t are invariants and only the linear mean velocity profile is a self-similar solution

$$\bar{u}_1 = \frac{b_1}{a_3} x_2 + C_4. \tag{3.33}$$

This profile applies in the viscous sublayer where ν/u_τ and u_τ are the symmetry-breaking length and velocity scales respectively. Another example is the turbulent Couette flow, where the symmetry is broken due to the moving wall velocity and channel height. Both cases will be discussed in § 4.

3.4. *Scaling laws of turbulent shear flows with non-zero system rotation*

Here, the symmetries of the equations (2.7*b*), (2.11) and (2.12) with $\Omega \neq 0$ are considered. The infinitesimal generators obtained are very similar to those in (3.19), with two differences. The most important difference is that

$$a_4 = 0 \tag{3.34}$$

is obtained and hence the scaling symmetry with respect to the time is lost. In addition, a new term $-2x_2\Omega b_1$ appears in η_p; this term corresponds to the fact that there is a radial pressure gradient due to rotation.

Except that the scaling symmetry with respect to a_4 is lost, the result is almost the same as the algebraic scaling law (3.27) with $c_2 = 0$

$$\bar{u}_1 = C_5 \Omega x_2 + C_6, \tag{3.35}$$

where the constants incorporate a collection of other constants. The linear law applies in the centre region of a rotating turbulent channel flow where the symmetry-breaking time scale is the inverse of the rotation rate Ω. The present case is distinguished from the previous linear mean velocity profiles, since a scaling of the spatial coordinates still holds ($a_1 \neq 0$). As a result, the length scale varies linearly in the region of its application, similar to the logarithmic region.

4. Experimental and numerical verification of the scaling laws

For any of the mean velocity profiles (3.27), (3.29), (3.31), (3.33) and (3.35), it is not obvious *a priori* that they exist in experimental or DNS data of turbulent flows. A proof of the fact that turbulence tends towards a high degree of symmetry if initial and boundary conditions are consistent is still lacking, even though such mean velocity profiles are found in innumerable experiments. In this section, experimental and DNS data will be used to give empirical verification of the different scaling laws.

Some of the mean velocity profiles derived in the previous section have been obtained previously by other methods and verified in several experiments and DNS data. The best known result is von Kármán's logarithmic law of the wall which

has been verified in a large number of experiments since its derivation. Another well-known mean velocity profile, derived in the previous section, is the linear mean velocity which may be found in the viscous sublayer of the universal law of the wall, and it is valid up to about $y^+ = 4$.

Beside the latter two cases all other flow profiles will be investigated in the following subsections. The first is the verification of the exponential law, which has never been reported in the literature. This has been found to match a broad region in the outer part of a turbulent boundary layer flow. The second one is the algebraic law, which fits about 80% of the core region of the turbulent channel flow. In addition, the algebraic scaling law has also been identified in the vicinity of the wall in low Reynolds number DNS data of a turbulent channel flow. The third is the linear mean velocity profile matching a broad region in a rotating channel flow. The slope of the linear part scales with the rotation rate. The final test case is the plane Couette flow which also exhibits a large linear section in the centre of the mean velocity profile. Both the latter linear profiles are physically very distinct from each other since they have different symmetry properties.

4.1. *Zero pressure-gradient turbulent boundary layer flow*

There is a considerable amount of data available for canonical boundary layer flows (Gad-el-Hak & Bandyopadhyay 1994; Fernholz & Finley 1996), but the data are generally for low Reynolds number and some contain too much scatter. For the present purpose the data need to be very smooth. To avoid misinterpretation of the results, extensive time averaging is required. This is because the velocity, rather than the wall distance, will be plotted with logarithmic scaling. Due to the logarithmic scaling of the y-axis, errors for small values of y are critical and may lead to wrong conclusions.

Three sets of experimental data have been chosen for comparison with the exponential velocity profile. These data are at medium to high Reynolds numbers, and we believe that they have been taken very carefully. The data of D. DeGraaff (1996, personal communication) are very smooth and cover the Reynolds number range $Re_\theta = 1500$–$20\,000$, where $\theta = \int_0^\infty (1 - \bar{u}/\bar{u}_\infty)\bar{u}/\bar{u}_\infty \, \mathrm{d}y$ is the momentum thickness and $\bar{u}_\infty$ is the free-stream velocity. The second set of data is from Fernholz *et al.* (1995) with the highest Reynolds number of $Re_\theta = 60\,000$. The third data set, from Saddoughi & Veeravalli (1994), reaches the highest available Reynolds number in a laboratory of $Re_\theta = 370\,000$.

Figure 1 shows DeGraaff's data for the mean velocity profiles taken at six different Reynolds numbers, in the usual wall variables in semi-log scaling. The extent of the viscous subregion and the logarithmic region are visible, with extent depending on the Reynolds number. In outer scaling the log region extends approximately to $y/\Delta = 0.025$ where $\Delta = \int_0^\infty (\bar{u}_\infty - \bar{u})/u_\tau \, \mathrm{d}y$ is the Rotta–Clauser length scale and u_τ is the friction velocity.

As has been pointed out above, there are strong indications that the exponential law (3.31*a*) matches the outer part, the wake, of a high Reynolds number flat-plate boundary layer flow, the reason being twofold. First, the usual law of the wake or velocity defect law $(\bar{u}_\infty - \bar{u}_1)/u_\tau = f(y/\delta)$ may be written in the form (3.31) by solving for $\bar{u}_1$ where δ is a characteristic boundary layer thickness. Second, and most important, it is the classical assumption that the macro length scale, such as the integral length scale, is a constant in the domain of applicability of the wake law. It is the symmetry breaking of the scaling of space by a constant length scale which in fact led in § 3.3.3 to the exponential mean velocity profile (3.31).

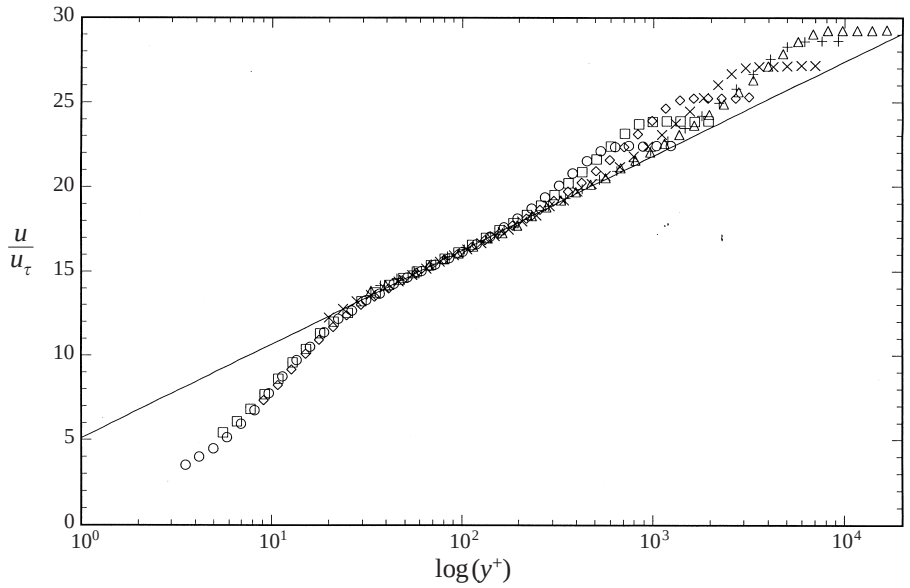

FIGURE 1. Mean velocity of the zero-pressure-gradient turbulent boundary layer in log-linear scaling from DeGraaff (1996): ○, $Re_\theta = 1500$; □, $Re_\theta = 2300$; ◇, $Re_\theta = 3800$; ×, $Re_\theta = 8600$; +, $Re_\theta = 15\,000$; △, $Re_\theta = 20\,000$; ——, $2.41\ln(y^+) + 5.1$.

In order to match the result from the theoretical approach and the data, the exponential mean velocity profile in equation (3.31*a*) will be re-written in outer scaling

$$\frac{\bar{u}_\infty - \bar{u}}{u_\tau} = \alpha \exp\left(-\beta \frac{y}{\Delta}\right), \tag{4.1}$$

where α and β are universal constants.

In figure 2 the turbulent boundary layer data are plotted as $\log[(\bar{u}_\infty - \bar{u})/u_\tau]$ vs. y/Δ. If the data match the scaling law given by (4.1) they would fall on a straight line. In the scaling of figure 2 the log region is valid up to $y/\Delta \approx 0.025$ and does not follow the exponential (4.1). For all Reynolds number cases, there is no Reynolds number dependence within the measurement accuracy, and all the data appear to converge to a straight line in the region $y/\Delta \approx 0.025 - 0.15$. The data of Saddoughi & Veeravalli (1994) show a longer region for the exponential law up to about $y/\Delta \approx 0.23$. With increasing Reynolds number the applicability of the exponential law appears to increase. For the medium Reynolds number cases, the applicability is approximately five to six times longer than the logarithmic law and for the high Reynolds number case it is about eight to nine times longer.

The outer part of the boundary layer does not match the exponential (4.1) and it appears that a weak Reynolds number dependence exists. This seems to be in contradiction to results of Coles (1962) who found the wake parameter to be constant for $Re_\theta > 5000$. However, several explanations can be given for this behaviour. It is common to have a few percent of error in experimental data. Since the data are plotted in log coordinates, and the free-stream velocity is subtracted, a few percent error in the free-stream velocity has a large impact on the lower part of the curve. This is almost invisible in the upper part. In fact from $y/\Delta \approx 0.3$ the data for the medium

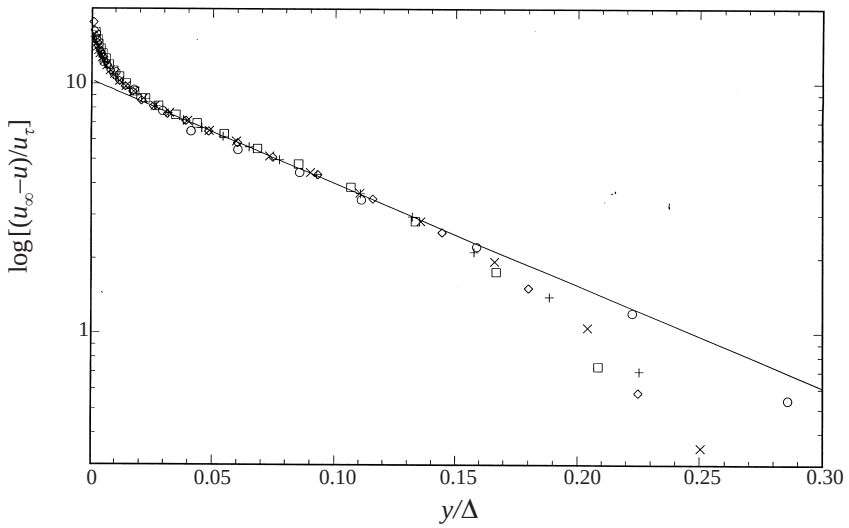

FIGURE 2. Mean velocity of the zero-pressure-gradient turbulent boundary layer in linear-log scaling of the defect law: ○, $Re_\theta = 370\,000$ (Saddoughi & Veeravalli 1994); □, and ◇, $Re_\theta = 60\,000$ (Fernholz *et al.* 1995); +, $Re_\theta = 15\,000$ and ×, $Re_\theta = 20\,000$ (DeGraaff 1996); ———, $10.34\exp(-9.46y/\Delta)$.

Reynolds number flows exhibit no clear trend. This is due to the error accumulation coming from the difference of two almost equally large numerical values.

The value $y/\Delta \approx 0.3$ corresponds approximately to the boundary layer edge. It is also possible that the outer-region large-scale intermittency plays a dominant role for the scaling of the mean velocity.

If the exponential velocity profile (4.1) were valid over the entire boundary layer, integration of (4.1) from zero to infinity would give $\alpha = \beta$. A least-square fit approximates the latter equivalence with $\alpha = 10.34$ and $\beta = 9.46$.

Even though the exponential (4.1) in figure 2 shows an excellent agreement with the experimental data, one may object that, unlike the channel flow, boundary layer flows are not strictly fully parallel flows. However, since the streamline curvature is usually very small, the flow may be considered as locally parallel. The dependence on the streamwise position is accounted for by the Rotta–Clauser length Δ and hence does not appear in the experimental results explicitly.

4.2. *The two-dimensional turbulent channel flow*

Most data for the turbulent channel flow exhibit too much scatter and cannot be used for the present purpose. A fair comparison between data and an algebraic law may only be made in log-log plots. Here the experimental data of Niederschulte (1996), Wei & Willmarth (1989) and the low Reynolds number DNS data of Kim, Moin & Moser (1987) will be used for the investigation of the algebraic scaling law.

Due to their simplicity, algebraic scaling laws have been traditionally used in fluid-engineering applications to fit mean profiles in turbulent boundary layer data. A well known example is the 1/7-law for the turbulent pipe flow (Schlichting 1979).

Here another algebraic regime is found where the origin of the independent coordinate is not the wall but rather the centre of the channel. The region of validity of an algebraic scaling law near the centre-line appears to be more clear than for the near-wall region. The reason for that may be found in the infinitesimal generators (3.19). Since for the algebraic scaling law, both constants a_1 and a_4 have to be non-zero and

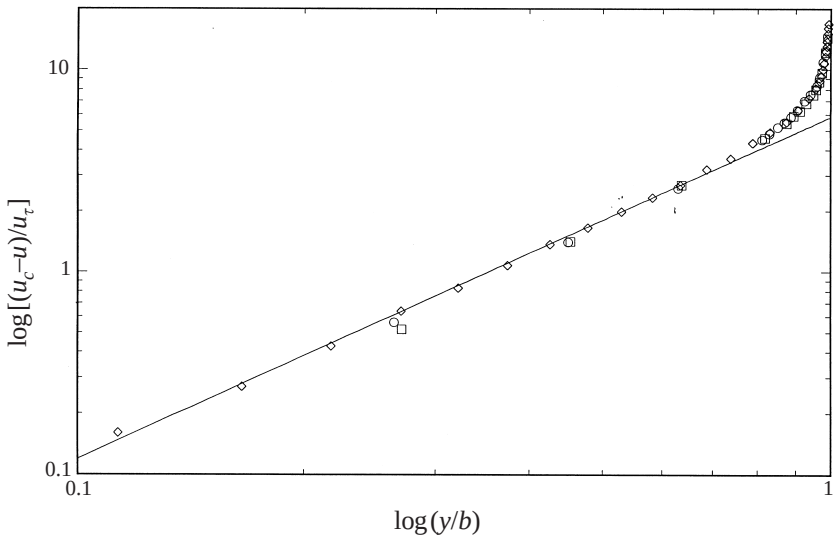

FIGURE 3. Mean velocity of the turbulent channel flow in log-log defect law scaling: ○, $Re_c = 40\,000$; □, $Re_c = 23\,000$ Wei & Willmarth (1989); ◇, $Re_c = 18\,000$ Niederschulte (1996); ———, $5.83(y/b)^{1.69}$.

distinct, the region for which the algebraic scaling law applies has the highest degree of symmetry. The centre region seems to be more suitable for that; in the near-wall region, u_τ is symmetry breaking, which results in $a_1 = a_4$ and eventually leads to the log law.

Regarding the algebraic law in the centre of the channel, the appropriate outer scaling for the channel is similar to the turbulent boundary layer flow

$$\frac{\bar{u}_c - \bar{u}}{u_\tau} = \varphi \left(\frac{y}{b}\right)^\gamma, \tag{4.2}$$

where φ and γ are constants, y originates on the channel centreline, $\bar{u}_c$ is the centreline velocity and b is the channel half-width.

In figure 3 the data of Wei & Willmarth (1989) and Niederschulte (1996) have been plotted in log-log scaling for the Reynolds number range $Re_c = 18\,000$–$40\,000$, where Re_c is based on the centreline velocity and channel half-width. Even though the data exhibit some scatter, there is a clear indication that the centre region up to about $y/b = 0.8$ closely follows an algebraic scaling law given by (4.2). The unknown constants in (4.2) have been fitted to $\varphi = 5.83$ and $\gamma = 1.69$ using Niederschulte's data. We believe that Niederschulte's experiment has been done very carefully and the algebraic scaling law extends a long way towards the centreline.

An even more profound indication regarding the algebraic law may be obtained from the DNS data of Kim *et al.* (1987). In figure 4, the data are plotted with log-log scaling and an almost perfectly straight line is visible for both $Re_c = 3300$ and 7900 from the centreline up to about $y/b = 0.75$. The scaling extends slightly further out for the $Re_c = 7900$ case. Since both Reynolds numbers in the DNS are low, a weak Reynolds number dependence of both φ and γ exists.

At this point it may be instructive to refer to a recent result of Oberlack (1999) who analysed circular parallel turbulent shear flows with respect to the self-similarity using the present approach. For this case he also found the existence of an algebraic

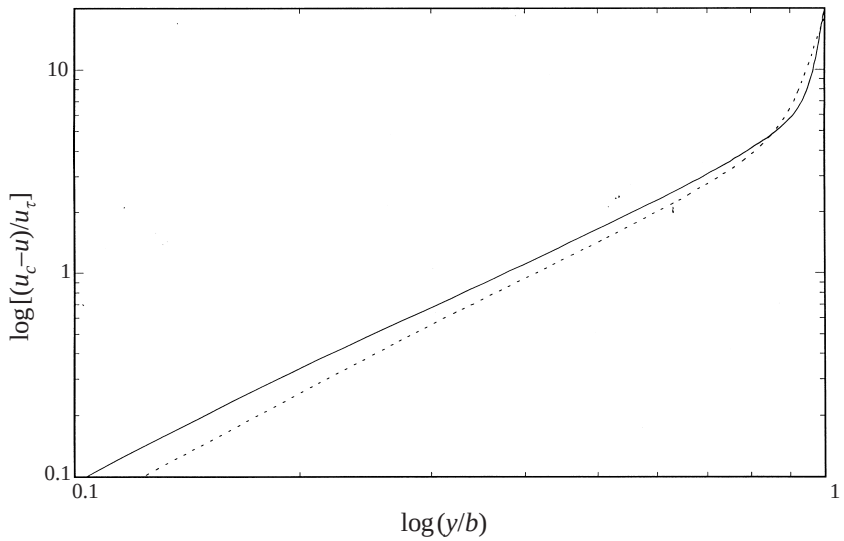

FIGURE 4. Mean velocity of the turbulent channel flow in double-log defect-law scaling from Kim *et al.* (1987): ——, $Re_c = 7900$; – – –, $Re_c = 3300$.

scaling law. Oberlack analysed the high Reynolds number data of Zagarola (1996) and found an almost perfect fit, covering 80% of the centre of the pipe.

In Appendix B the two-point correlation equations have been analysed with respect to their self-similarity for a parallel shear flow. The resulting equation for the mean flow (B 9) is fully equivalent to (3.24*a*). New scaling laws for the two-point correlations are obtained.

Hunt *et al.* (1987) have analysed the two-point correlations with respect to self-similarity using the data of Kim *et al.* (1987). They investigated the near-wall region assuming the logarithmic law to hold. The surprising result here is that the self-similarity of R_{22} extends much further towards the centreline than might be expected from the fairly short extent of the log region in the mean flow. The result could be clarified using the fact that the near-wall region does not follow a log, but rather an algebraic, scaling law. Figure 5 shows the mean velocity of the channel flow data in log-log coordinates. Up to about $y^+ = 4$ the linear law of the viscous sublayer is valid. In the range $50 < y^+ < 250$ for $Re_c = 7900$ an almost perfectly straight line is visible and a least-square fit of an algebraic law in this range results in a much higher correlation coefficient than a least-square fit of a logarithmic function. Since the algebraic law extends much further than a logarithmic law, it is also expected that the self-similarity of the two-point correlation R_{22} holds much further. The only difference for R_{22} regarding the two different scaling laws is that, in case of the algebraic scaling law, R_{22} also scales with the wall distance, while for the log law, this is not the case, as may be deduced from equation (B 13).

4.3. *The rotating two-dimensional turbulent channel flow*

System rotation is known to have a strong influence on turbulence. With increasing rotation rate a turbulent flow tends to become more two-dimensional while the axis of independence is aligned with the rotation vector. As a consequence, the mean velocity is also significantly affected as for example in the present case of a rotating two-dimensional channel flow where the rotation axis is parallel to the mean vorticity

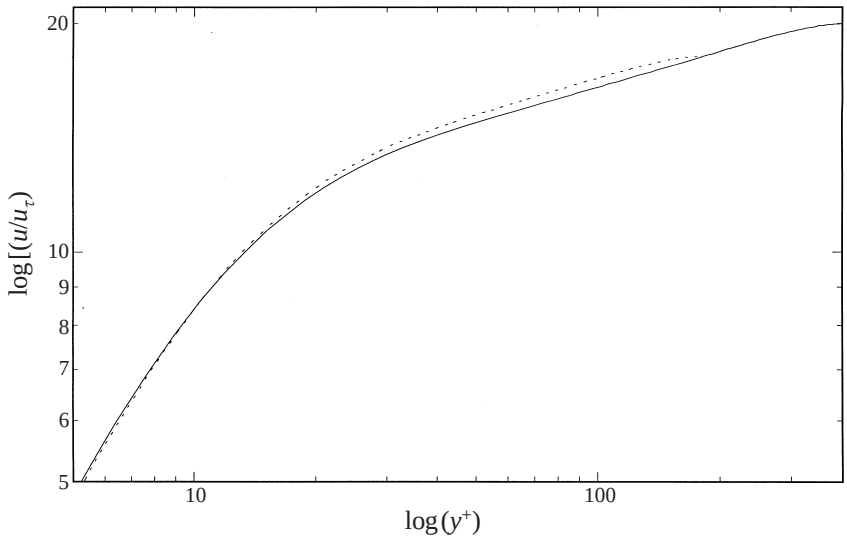

FIGURE 5. Mean velocity of the turbulent channel flow in log-log scaling from Kim *et al.* (1987): ——, $Re_c = 7900$; – – –, $Re_c = 3300$.

vector. Compared to the non-rotating channel flow, which exhibits the highest degree of symmetry in the centre region of the flow, here the external time scale Ω^{-1} is symmetry breaking which leads to $a_4 = 0$. This affects in particular the centre region of the flow which appears to become linear. This result can also be obtained from employing $a_4 = 0$ in equation (3.24). However, in contrast to the turbulent Couette flow, to be discussed in the following subsection, a scaling symmetry with respect to the spatial coordinates still exists ($a_1 \neq 0$).

An early experimental investigation of the present flow problem has been done by Johnston, Halleen & Lazius (1972) who obtained a linear centre region at sufficiently high rotation rates. Equation (3.35*a*) may be rewritten as

$$\bar{u}_1 = \sigma_1 \Omega x_2 + \sigma_2. \tag{4.3}$$

A recent DNS of Kristoffersen & Andersson (1993) also confirmed this form of the mean velocity profiles. Their results are shown in figure 6 for two different rotation rates. The data are presented employing the rotation number $Ro = 2|\Omega|h/\bar{u}_m$, a non-dimensional measure of the rotation rate. Both Johnston *et al.* (1972) and Kristoffersen & Andersson (1993) found the slope coefficient in (4.3) to be $\sigma_1 \approx 2$.

It has already been recognized in the literature that that value coincides with zero absolute vorticity $2\Omega - \mathrm{d}\bar{u}_1/\mathrm{d}x_2$. An additional feature of this particular value for σ_1 is that the linear region of the flow becomes neutrally stable. An overview on the literature regarding these flow characteristics is given in Kristoffersen & Andersson (1993).

4.4. *The turbulent plane Couette flow*

Even though a linear mean velocity profile is also obtained for the present flow it is very distinct from the previous test case. Here, the lowest degree of symmetry is considered where a length and a velocity scale dominate the flow and both scaling symmetries in (3.24) are broken ($a_1 = a_4 = 0$). Hence, comparing to (4.3), scaling with respect to the spatial coordinate is also lost. It appears that the present case applies

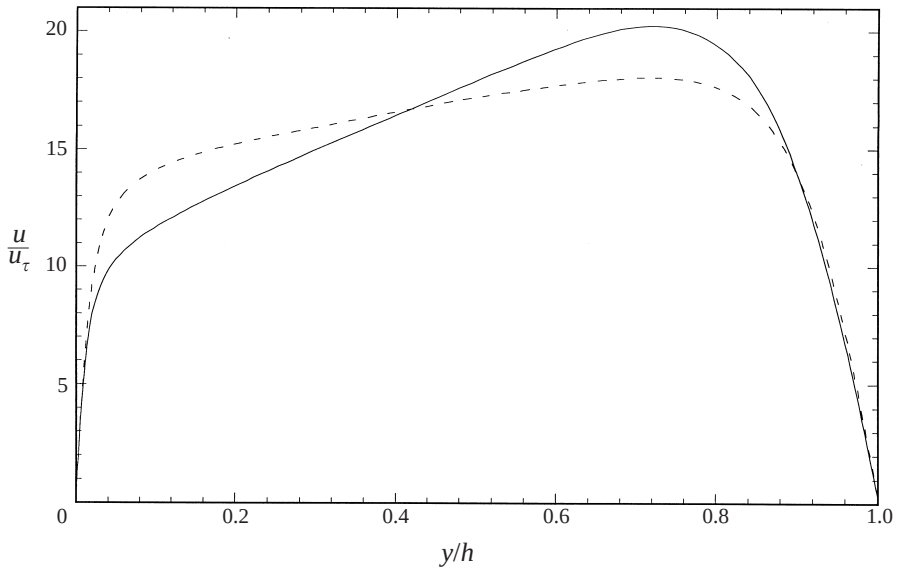

FIGURE 6. Mean velocity of the rotating two-dimensional turbulent channel flow from Kristoffersen & Andersson (1993): – – –, $Ro = 0.2$; ——, $Ro = 0.5$.

to the turbulent plane Couette flow. The mean velocity may be written as

$$\bar{u}_1 = \vartheta_1 \frac{u_w}{h} x_2 + \vartheta_2, \tag{4.4}$$

where h and u_w are the channel half-width and the wall velocity, respectively, and ϑ_1 and ϑ_2 are constants.

Several experimental and numerical investigations of the plane Couette flow have been reported in the literature. An overview on the literature is given in Bech *et al.* (1995). The experimental work by El Telbany & Reynolds (1980) and the DNS data by Lee & Kim (1991) have been depicted in figure 7. With relatively high accuracy about 80% of the centre region is fitted by the linear mean velocity profile. The slopes of experimental and numerical results appear to be slightly different. This may be a Reynolds number effect since both data sets are taken at different and comparably low Reynolds numbers. In the near-wall region other scaling laws become dominant.

As already mentioned, a second linear mean velocity profile, which is also dominated by two external scales, is the viscous sublayer. Here, the scales are ν/u_τ and u_τ, the viscous length scale and the friction velocity, respectively. This case is very well know and can be verified in figure 5.

5. Discussion and conclusions

It has been demonstrated by the application of Lie group ideas to plane parallel turbulent shear flows that a large class of solutions for the mean velocity can be computed. These flow profiles include the logarithmic law of the wall, an algebraic law, and a linear profile; a new exponential mean profile has also been found.

Two different aspects of the present approach are distinct from earlier investigations seeking self-similar flow profiles in parallel shear flows. First, using Lie group analysis, it is guaranteed that all self-similar solutions of the equation under investigation will be obtained. The Lie group approach also covers all results derived from dimensional

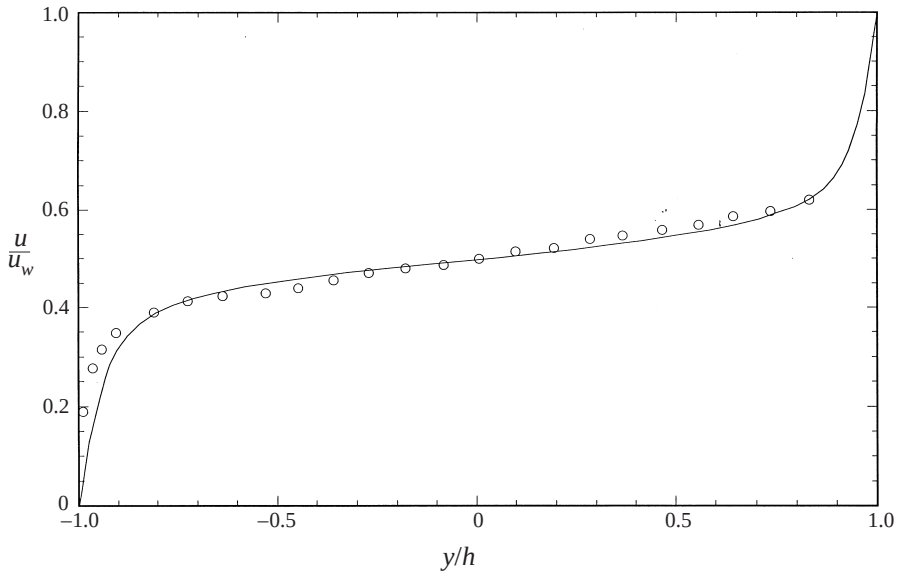

FIGURE 7. Mean velocity in turbulent plane Couette flow: ○, El Telbany & Reynolds (1980); ———, Lee & Kim (1991).

analysis (Bluman & Kumei 1989). The theory is fully algorithmic and no intuition is needed to find a self-similar mean velocity profile.

Second, the underlying equations used in the present approach are not the mean momentum and the Reynolds stress equations, as used in many previous investigations (Townsend 1976). Instead, symmetries in the set of equations consisting of the equations for the velocity fluctuations (2.11), and the velocity product equations (2.12) are analysed. The approach based on these equations has the following advantage: as shown in Appendix A their invariance is a sufficient condition to have all the flow profiles consistent with all higher-order correlation equations.

However, the converse is not true. There is still a small likelihood of the second-order and higher correlation equations admitting certain symmetries which are not detected by the present approach. This point bears further investigation.

Using DNS and experimental data the exponential and algebraic laws have been demonstrated to be valid in the outer part of boundary layer and channel flows respectively. For the turbulent boundary layer, high-quality data are available, and there is little doubt regarding the existence of an exponential region. For the turbulent channel flow, the DNS data exhibit an almost perfect algebraic centre region, but the data are at low Reynolds number and show Reynolds number dependence of the scaling law parameters. The experimental data also clearly show the algebraic region, but contain more scatter.

One may argue that a channel flow is not an appropriate example for the algebraic scaling law since in its derivation no external time or velocity scales are allowed. The underlying reason from Lie group analysis has been discussed in some detail in § 3. In a turbulent channel flow, the length and the velocity scales are given by the channel width and the friction velocity respectively. However, from the data presented, it is quite clear that the algebraic law is valid in the centre of a channel flow. Using this experimental result, one may draw the following conclusion, which also holds for the other scaling laws: All the scaling laws have a limited range of applicability. Beyond

a certain limit, a scaling law does not 'feel' the length, time or velocity scale locally imposed on some region of the flow, and a higher degree of symmetry may be reached if no other restriction applies. In case of the channel flow, the algebraic scaling law is embedded between two log regions. Neither the friction velocity nor the channel width is symmetry breaking.

Another algebraic scaling law in the vicinity of the wall has already been derived by Barenblatt (1993) and George *et al.* (1993). It has also been computed in the present investigation and could be confirmed using the low Reynolds number DNS data of Kim *et al.* (1987).

Three linear mean velocity profiles have been identified in experimental and in DNS data. It appears that from a symmetry point of view the well-known viscous sublayer and the turbulent Couette flow have similar group characteristics. In both cases a length and a velocity scale is symmetry breaking. Data for a rotating channel flow exhibit a third linear mean velocity profile with its slope scaling with Ω. This profile is distinct from the two other cases since only one scaling symmetry with respect to the time is lost: a scaling symmetry with respect to the spatial coordinate still exists.

In Appendix B all results for the mean flow have also been derived by applying the Lie symmetry approach to the two-point correlation equations. For the two-point correlation tensor an empirical finding of Hunt *et al.* (1987) has been confirmed. They found self-similarity of the two-point correlation tensor in the vicinity of the wall and assumed that this corresponds to the log region. However, in § 4 it was shown that the region they have analysed is more likely to be an algebraic region. Nevertheless, the present findings are in full agreement with their observations.

It may be concluded from the present analysis and some results for cylindrical flows (Oberlack 1999) that a high degree of symmetry is a preferred state of turbulence if allowed by initial and boundary conditions. This observation appears to be a fundamental property of turbulence and the following working hypothesis may be formulated:

HYPOTHESIS: *The mean velocity $\bar{u}_i$ in an incompressible turbulent flow establishes a maximum degree of symmetry consistent with the equations* (2.5)–(2.7) *and* (2.12) *and the initial and the boundary condition.*

The hypothesis is formulated in a very general form. It could be argued that it is too optimistic to think that this hypothesis holds for a more complex flow. However, one should keep in mind that the present approach was restricted to a plane and parallel flow. Relaxing this limitation will eventually result in much more general flows as has already been shown by Oberlack (1999).

An important application of the present approach is turbulence modelling. Many common statistical turbulence models may not be consistent with all the symmetries calculated in the present approach and hence will not capture the associated scaling laws. As an example consider the standard k–ε model which, interestingly, formally admits all symmetries of the time-dependent three-dimensional Navier–Stokes equations (see Khor'kova & Verbovetsky 1995). This is somewhat misleading, since this does not guarantee the correct behaviour for lower dimensional cases such as plane shear flows.

The standard k-ε model captures some non-trivial scaling laws, such as the exponential law. However, it may be shown that in the case of a turbulent rotating channel flow the symmetry groups of the k–ε model are not consistent with the present finding. As a result, this model misses the correct linear region in the centre of the

channel flow. In fact, the inability of the k–ε model to properly predict the rotating channel flow can be traced back to too many symmetries. In § 3.4 it was shown that the rotation rate Ω is symmetry breaking for the scaling of time which leads to the linear region. By contrast, scaling of time is still admitted by the k–ε model even when rotation is present.

These findings may be used to develop new or improve existing turbulence models. We propose that turbulence models should have the symmetry properties computed in the present analysis. This is a necessary condition in order to capture the turbulent scaling laws and the associated turbulent flows present herein. The presented symmetry properties in turbulent flows may be considered as a new realizability concept.

A fundamental question which could not be resolved so far is why turbulence relaxes to a self-similar mean velocity profile under certain boundary and initial conditions. Heuristically speaking, self-similar flow profiles are those solutions which may be expressed by a lower number of independent variables. It appears that, in certain regions, turbulence has some tendency towards a low-dimensional state for the mean quantities. In addition the fundamental mechanism which fixes the constants in the scaling laws is still unknown. The constants in the scaling laws appear to be universal for high Reynolds number flows. Furthermore, there may be some relation between certain constants. A semi-empirical approach has been developed by Roth (1970) to find a relation between von Kármán's and Kolmogorov's constants. These and other questions will be the topic of future research.

The author is very much indebted to Thomas R. Bewley, Peter Bradshaw, Brian J. Cantwell, William K. George, Nail H. Ibragimov, Krishnan Mahesh, William C. Reynolds and Seyed G. Saddoughi for giving valuable comments. The author is in particular thankful to Javier Jimenez for discussing some physical interpretations of the symmetry groups. Furthermore he thanks Dave DeGraaff, Robert D. Moser, Seyed G. Saddoughi, Martin Schober and Timothy Wei for the kind cooperation and their provision of the data. Finally, he would like to thank Willy Hereman who was extremely patient in answering all questions regarding the Lie group package SYMMGRP.MAX. The work was in part supported by the Deutsche Forschungsgemeinschaft under grant number Ob 96/2-1.

Appendix A. Proof of consistency with higher-order velocity product equations

It will be shown that the generators (3.19) are not only consistent with the equations for second-order velocity product $u_i u_j$, but also with the equations for all higher-order velocity products $u_{i_1} u_{i_2} \dots u_{i_{n-1}} u_{i_n}$. As a result all flow profiles derived in the present paper are also solutions of all higher-order velocity product equations.

The equation for the velocity product of any arbitrary order n is given by

$$\mathscr{M}_{i_1 i_2 \dots i_{n-1} i_n} = u_{i_1} u_{i_2} \cdot \dots \cdot u_{i_{n-1}} \mathscr{N}_{i_n} + u_{i_1} u_{i_2} \cdot \dots \cdot u_{i_{n-2}} \mathscr{N}_{i_{n-1}} u_{i_n} + \dots + u_{i_1} \mathscr{N}_{i_2} u_{i_3} \cdot \dots \cdot u_{i_{n-1}} u_{i_n} + \mathscr{N}_{i_1} u_{i_2} \cdot \dots \cdot u_{i_{n-1}} u_{i_n} = 0. \tag{A 1}$$

The twice prolongated operator (3.11) together with the generators (3.19) may be written as

$$\mathrm{X} = (a_1 - a_4) u_j \frac{\partial}{\partial u_j} + \hat{\mathrm{X}} \tag{A 2}$$

where $\hat{\mathrm{X}}$ contains all other derivatives with respect to the remaining variables in (3.4) and also all prolongations.

All higher-order velocity product equations (A 1) are consistent with the mean velocity profiles given in § 3 if the operator (A 2) applied to equation (A 1) is identically zero.

To show this, the operator (A 2) will be applied to equation (A 1). Using (3.12*b*) and noting that $\hat{\mathrm{X}}$ in the operator (A 2) does not act on u_l, one may verify that

$$\mathrm{X}\mathscr{M}_{i_1 i_2 \ldots i_{n-1} i_n} = (u_{i_1} u_{i_2} \cdot \cdots \cdot u_{i_{n-1}} \mathscr{N}_{i_n} + u_{i_1} u_{i_2} \cdot \cdots \cdot u_{i_{n-2}} \mathscr{N}_{i_{n-1}} u_{i_n} + \cdots + u_{i_1} \mathscr{N}_{i_2} u_{i_3} \cdot \cdots \cdot u_{i_{n-1}} u_{i_n} + \mathscr{N}_{i_1} u_{i_2} \cdot \cdots \cdot u_{i_{n-1}} u_{i_n})(a_1 - a_4)(n-1). \tag{A 3}$$

Since (A 3) can be combined with (A 1) it is obvious that the latter equation is identically zero.

Appendix B. Two-point correlation approach

A similar approach to analyse symmetries in parallel shear flows can be made by investigating the two-point correlation equations given by

$$\begin{aligned} \frac{\mathrm{D}R_{ij}}{\mathrm{D}t} = & -R_{kj} \frac{\partial \bar{u}_i(\boldsymbol{x},t)}{\partial x_k} - R_{ik} \left. \frac{\partial \bar{u}_j(\boldsymbol{x},t)}{\partial x_k} \right|_{\boldsymbol{x}+\boldsymbol{r}} - [\bar{u}_k(\boldsymbol{x}+\boldsymbol{r},t) - \bar{u}_k(\boldsymbol{x},t)] \frac{\partial R_{ij}}{\partial r_k} \\ & - \left[\frac{\partial \overline{pu_j}}{\partial x_i} - \frac{\partial \overline{pu_j}}{\partial r_i} + \frac{\partial \overline{u_i p}}{\partial r_j} \right] + \nu \left[\frac{\partial^2 R_{ij}}{\partial x_k \partial x_k} - 2 \frac{\partial^2 R_{ij}}{\partial x_k \partial r_k} + 2 \frac{\partial^2 R_{ij}}{\partial r_k \partial r_k} \right] \\ & - \frac{\partial R_{(ik)j}}{\partial x_k} + \frac{\partial}{\partial r_k} [R_{(ik)j} - R_{i(jk)}] - 2\Omega_k [e_{kli} R_{lj} + e_{klj} R_{il}], \end{aligned} \tag{B 1}$$

where

$$\left. \begin{aligned} R_{ij}(\boldsymbol{x},\boldsymbol{r}) &= \overline{u_i(\boldsymbol{x})\, u_j(\boldsymbol{x}')}, \\ R_{(ik)j}(\boldsymbol{x},\boldsymbol{r}) &= \overline{u_i(\boldsymbol{x})\, u_k(\boldsymbol{x})\, u_j(\boldsymbol{x}')}, \quad R_{i(jk)}(\boldsymbol{x},\boldsymbol{r}) = \overline{u_i(\boldsymbol{x})\, u_j(\boldsymbol{x}')\, u_k(\boldsymbol{x}')}, \\ \overline{pu_j}(\boldsymbol{x},\boldsymbol{r}) &= \overline{p(\boldsymbol{x})\, u_j(\boldsymbol{x}')}, \quad \overline{u_j p}(\boldsymbol{x},\boldsymbol{r}) = \overline{u_j(\boldsymbol{x})\, p(\boldsymbol{x}')}, \end{aligned} \right\} \tag{B 2}$$

and $\mathrm{D}/\mathrm{D}t = \partial/\partial t + \bar{u}_k \partial/\partial x_k$. The tensors in (B 2) are functions of the physical and the correlation space coordinates, $\boldsymbol{x}$ and $\boldsymbol{r} = \boldsymbol{x}' - \boldsymbol{x}$ respectively.

The divergences $\partial/\partial x_i - \partial/\partial r_i$ and $\partial/\partial r_j$ applied to (B 1) yield the two-point pressure–velocity correlation equations,

$$\begin{aligned} \frac{\partial^2 \overline{pu_j}}{\partial x_k \partial x_k} - 2\frac{\partial^2 \overline{pu_j}}{\partial r_k \partial x_k} + \frac{\partial^2 \overline{pu_j}}{\partial r_k \partial r_k} = & -2 \left[\frac{\partial \bar{u}_k(\boldsymbol{x},t)}{\partial x_l} + e_{mlk}\Omega_m \right] \left[\frac{\partial R_{lj}}{\partial x_k} - \frac{\partial R_{lj}}{\partial r_k} \right] \\ & - \left[\frac{\partial^2 R_{(kl)j}}{\partial x_k \partial x_l} - 2\frac{\partial^2 R_{(kl)j}}{\partial x_k \partial r_l} + \frac{\partial^2 R_{(kl)j}}{\partial r_k \partial r_l} \right] \end{aligned} \tag{B 3}$$

and

$$\frac{\partial^2 \overline{u_i p}}{\partial r_k \partial r_k} = -2 \left[\left. \frac{\partial \bar{u}_k(\boldsymbol{x},t)}{\partial x_l} \right|_{\boldsymbol{x}+\boldsymbol{r}} + e_{mlk}\Omega_m \right] \frac{\partial R_{il}}{\partial r_k} - \frac{\partial^2 R_{i(kl)}}{\partial r_k \partial r_l} \tag{B 4}$$

respectively.

The vertical lines in (B 1) and (B 4) denote that the derivatives are taken with respect to $\boldsymbol{x}$, and evaluated at $\boldsymbol{x}+\boldsymbol{r}$. It is this non-local behaviour of the mean velocity which makes it difficult to apply two-point correlations to inhomogeneous flows.

For the derivation of a non-parametric symmetry in the two-point correlation equations, the following two identities are needed. They may be derived from a geometrical consideration by interchanging the two points $\boldsymbol{x}$ and $\boldsymbol{x}' = \boldsymbol{x} + \boldsymbol{r}$; i.e.

$$R_{ij}(\boldsymbol{x}, \boldsymbol{r}; t) = R_{ji}(\boldsymbol{x} + \boldsymbol{r}, -\boldsymbol{r}; t), \tag{B 5a}$$

$$\overline{u_i p}(\boldsymbol{x}, \boldsymbol{r}; t) = \overline{p u_i}(\boldsymbol{x} + \boldsymbol{r}, -\boldsymbol{r}; t). \tag{B 5b}$$

A similar identity may be derived for the triple correlation.

B.1. *Symmetries in the two-point correlation equations*

The symmetries and results for the mean velocity profiles may also be derived by means of the two-point correlation equations. In addition, some new results for the two-point correlation tensor are obtained.

For this purpose, a small modification of the approach used in § 3 is introduced. The mean velocity $\bar{u}_1$ is not considered a variable in the infinitesimal transformation, but is treated as an unknown function of x_2. This method is called group classification (see e.g. Ibragimov 1994/1995). Solving the equations for the infinitesimal generators, it turns out that an ODE for $\bar{u}_1$ is derived, which is equivalent to the ODE for $\bar{u}_1$ given in equation (3.24*a*).

The general problem when applying Lie group methods to the two-point correlation equation is the coupling of the second moments to the infinite number of higher-order correlations. Of course, this cannot be taken into account in the symmetry calculation. A reduced system of equations is therefore analysed. From a mathematical point of view, the approach in this Appendix does not ensure that all the calculated symmetries are consistent with all higher-order correlations.

For the symmetries in the two-point correlation equation to follow, some simplifications have been introduced. Apart from the parallel flow assumption (2.8), only the inviscid equations will be considered. Using these restrictions, only the equations for R_{22} in (B 1), $\overline{pu_2}$ in (B 3) and $\overline{u_2 p}$ in (B 4) need to be examined, because these equations decouple from the other components in the tensor equations.

Equivalent to the approach in § 3, the symmetries of the 22-component of the equations (B 1)–(B 4) are derived by application of the operator

$$\begin{aligned} \mathrm{Y} = {} & \xi_{r_1}\frac{\partial}{\partial r_1} + \xi_{r_2}\frac{\partial}{\partial r_2} + \xi_{r_3}\frac{\partial}{\partial r_3} + \xi_{x_2}\frac{\partial}{\partial x_2} \\ & + \eta_{R_{22}}\frac{\partial}{\partial R_{22}} + \eta_{\overline{pu_2}}\frac{\partial}{\partial \overline{pu_2}} + \eta_{\overline{u_2 p}}\frac{\partial}{\partial \overline{u_2 p}} + \eta_{R_{(2k)2}}\frac{\partial}{\partial R_{(2k)2}} + \eta_{R_{2(2k)}}\frac{\partial}{\partial R_{2(2k)}}, \end{aligned} \tag{B 6}$$

and its second prolongation to the 22-component of the equations (B 1)–(B 4). This results in the generators

$$\left.\begin{aligned} & \xi_{r_1} = q_1 r_1 + q_2, \quad \xi_{r_2} = q_1 r_2, \quad \xi_{r_3} = q_1 r_3 + q_3, \quad \xi_{x_2} = q_1 x_2 + q_4, \\ & \eta_{R_{22}} = q_5 R_{22}, \quad \eta_{\overline{pu_2}} = q_6 \overline{pu_2}, \quad \eta_{\overline{u_2 p}} = q_6 \overline{u_2 p}, \\ & \eta_{R_{(2k)2}} = q_6 R_{(2k)2}, \quad \eta_{R_{2(2k)}} = q_6 R_{2(2k)}. \end{aligned}\right\} \tag{B 7}$$

As an additional result of solving the determining equations, a second-order ODE for the mean flow emerges, i.e.

$$\frac{\mathrm{d}^2 \bar{u}_1}{\mathrm{d}x_2^2}[q_1 x_2 + q_4] + \frac{\mathrm{d}\bar{u}_1}{\mathrm{d}x_2}[q_1 + q_5 - q_6] = 0 \tag{B 8}$$

since $\bar{u}_1$ was treated as an unknown function. Equation (B 8) can be integrated once to give

$$\frac{\mathrm{d}\bar{u}_1}{\mathrm{d}x_2}[q_1 x_2 + q_4] + \bar{u}_1[q_5 - q_6] = c. \tag{B 9}$$

It is equivalent to the ODE for $\bar{u}_1$ derived in (3.24).

The equations for the invariant surface are given by

$$\frac{\mathrm{d}r_1}{\xi_{r_1}} = \frac{\mathrm{d}x_2}{\xi_{x_2}}, \quad \frac{\mathrm{d}r_2}{\xi_{r_2}} = \frac{\mathrm{d}x_2}{\xi_{x_2}}, \quad \frac{\mathrm{d}r_3}{\xi_{r_3}} = \frac{\mathrm{d}x_2}{\xi_{x_2}}. \tag{B 10}$$

Taking $q_1 \neq 0$, the equations (B 10) are integrated and the constants of integration are taken as the new independent variables

$$\tilde{r}_1 = \frac{r_1}{x_2 + (q_4/q_1)}, \quad \tilde{r}_2 = \frac{r_2}{x_2 + (q_4/q_1)}, \quad \tilde{r}_3 = \frac{r_3}{x_2 + (q_4/q_1)}. \tag{B 11}$$

This corresponds to both the algebraic and the logarithmic law, (3.27) and (3.29) respectively. The new dependent variables are calculated by solving the three equations for the invariants

$$\frac{\mathrm{d}R_{22}}{\eta_{R_{22}}} = \frac{\mathrm{d}x_2}{\xi_{x_2}}, \quad \frac{\mathrm{d}\overline{pu_2}}{\eta_{\overline{pu_2}}} = \frac{\mathrm{d}x_2}{\xi_{x_2}}, \quad \frac{\mathrm{d}\overline{u_2 p}}{\eta_{\overline{u_2 p}}} = \frac{\mathrm{d}x_2}{\xi_{x_2}}, \quad \frac{\mathrm{d}R_{(2k)2}}{\eta_{R_{(2k)2}}} = \frac{\mathrm{d}x_2}{\xi_{x_2}}, \quad \frac{\mathrm{d}R_{2(2k)}}{\eta_{R_{2(2k)}}} = \frac{\mathrm{d}x_2}{\xi_{x_2}}, \tag{B 12}$$

where the constants of integration are taken as the new dependent variables:

$$R_{22} = \left(x_2 + \frac{q_4}{q_1}\right)^{q_5/q_1} \tilde{R}_{22}, \quad \overline{pu_2} = \left(x_2 + \frac{q_4}{q_1}\right)^{q_6/q_1} \widetilde{\overline{pu_2}}, \quad \overline{u_2 p} = \left(x_2 + \frac{q_4}{q_1}\right)^{q_6/q_1} \widetilde{\overline{u_2 p}},$$

$$R_{(2k)2} = \left(x_2 + \frac{q_4}{q_1}\right)^{q_6/q_1} \tilde{R}_{(2k)2}, \quad R_{2(2k)} = \left(x_2 + \frac{q_4}{q_1}\right)^{q_6/q_1} \tilde{R}_{2(2k)}. \tag{B 13}$$

If $q_5 = q_6$, then the log law holds, as may be deduced from equation (B 9). If $a_5 \neq a_6$, (B 9) may be integrated to an algebraic function.

Using the similarity coordinates (B 11) and (B 13) in (B 1), (B 3) and (B 4) and considering either the algebraic or the logarithmic scaling law, the dimension of the two-point correlation equations may be reduced by one.

When $q_1 = 0$, the exponential law holds and from (B 10) and (B 12) the new similarity variables can be integrated to obtain

$$\hat{r}_1 = r_1 + \frac{q_2}{q_4} x_2, \quad \hat{r}_2 = r_2, \quad \hat{r}_3 = r_3 + \frac{q_3}{q_4} x_2, \tag{B 14}$$

and

$$R_{22} = \mathrm{e}^{(q_5/q_4)x_2} \hat{R}_{22}, \quad \overline{pu_2} = \mathrm{e}^{(q_6/q_4)x_2} \widehat{\overline{pu_2}}, \quad \overline{u_2 p} = \mathrm{e}^{(q_6/q_4)x_2} \widehat{\overline{u_2 p}},$$

$$R_{(2k)2} = \mathrm{e}^{(q_6/q_4)x_2} \hat{R}_{(2k)2}, \quad R_{2(2k)} = \mathrm{e}^{(q_6/q_4)x_2} \hat{R}_{2(2k)}. \tag{B 15}$$

Introducing (B 15) into (B 1), (B 3) and (B 4), the number of independent variables is reduced by one.

Next, consider the classical log region which comprises the further restriction $q_4 = 0$. The identities (B 5) may be transformed in a similar manner. Oberlack (1995) has shown that this yields a non-local relation for R_{ij}. Introducing the transformation (B 11) into the equation (B 5*a*), the relation $R_{ij}(x_2, x_2\tilde{\boldsymbol{r}}) = R_{ji}(x_2(1 + \tilde{r}_2), -x_2\tilde{\boldsymbol{r}})$ is obtained. Assuming that all two-point correlation functions depend solely on the similarity variable (B 11), only the ratio of the first and the second parameters may

appear in this identity for R_{ij}. This argument may be extended to the pressure–velocity correlation. Thus, the final result is

$$R_{ij}(\tilde{\boldsymbol{r}}) = R_{ji}\left(\frac{-\tilde{\boldsymbol{r}}}{1+\tilde{r}_2}\right) \tag{B 16}$$

and

$$\overline{u_i p}(\tilde{\boldsymbol{r}}) = \overline{p u_i}\left(\frac{-\tilde{\boldsymbol{r}}}{1+\tilde{r}_2}\right). \tag{B 17}$$

The latter identity also holds if $\overline{u_i p}$ and $\overline{p u_i}$ are interchanged.

These two relations give insight into the structure of the solution. Relation (B 16) connects different $\tilde{\boldsymbol{r}}$ domains to each other and describes non-local behaviour in correlation space. This is useful, when interpreting two-point correlations in wall bounded flows, obtained from experimental or DNS data.

Note that the self-similar form of $R_{ij}(\tilde{\boldsymbol{r}})$ has been previously introduced by Hunt *et al.* (1987) as a working hypothesis when analysing DNS data of a low Reynolds number channel flow. Their study clearly validates the self-similarity of R_{ij} based on the similarity variables (B 11).

REFERENCES

Barenblatt, G. I. 1993 Scaling laws for fully developed turbulent shear flows. Part 1. Basic hypotheses and analysis. *J. Fluid Mech.* **248**, 513–520.

Bech, K. H., Tillmark, N., Alfredsson, P. H. & Andersson, H. I. 1995 An investigation of turbulent plane Couette flow at low Reynolds numbers. *J. Fluid Mech.* **286**, 291–325.

Bluman, G. W. & Kumei, S. 1989 *Symmetries and Differential Equations*. Applied Mathematical Sciences, vol. 81. Springer.

Cantwell, B. J. 1981 Organized motion in turbulent flows. *Ann. Rev. Fluid Mech.* **13**, 457–515.

Champagne, B., Hereman, W. & Winternitz, P. 1991 The computer calculation of Lie point symmetries of large systems of differential equations. *Comput. Phys. Comm.* **66**, 319–340.

Coles, D. 1962 The turbulent boundary layer in a compressible fluid. *Rep.* R-403-PR. The Rand Corporation, Santa Monica, CA.

Dellnitz, M., Golubitsky, M. & Melbourne, I. 1992 Mechanisms of symmetry creation. *Intl Series of Numer. Maths* **104**, 99–109.

El Telbany, M. M. M. & Reynolds, A. J. 1980 Velocity distributions in plane turbulent channel flows. *J. Fluid Mech.* **100**, 1–29.

Fernholz, H. H. & Finley, P. J. 1996 The incompressible zero-pressure-gradient turbulent boundary layer: an assessment of the data. *Prog. Aerospace Sci.* **32**, 245–311.

Fernholz, H. H., Krause, E., Nockemann, M. & Schober, M. 1995 Comparative measurements in the canonical boundary layer at $Re_{\delta_2} \leqslant 6 \times 10^4$ on the wall of the German–Dutch windtunnel. *Phys. Fluids* **7**, 1275–1281.

Field, M. & Golubitsky, M. 1995 Symmetric chaos: How and why. *Not. AMS* **42**(2), 240–244.

Gad-el-Hak, M. & Bandyopadhyay, P. R. 1994 Reynolds number effects in wall-bounded flows. *Appl. Mech. Rev.* **47**, no 8, 307–365.

George, W. K., Castillo, L. & Knecht, P. 1996 The zero pressure-gradient turbulent boundary layer. Tech. Rep. TRL-153. Turbulence Research Laboratory, School of Engineering and Applied Sciences, SUNY Bufallo, NY.

Hunt, J. C. R., Moin, P., Moser, R. D. & Spalart, P. R. 1987 Selfsimilarity of two-point correlation in wall bounded turbulent flows. *Proc. Center for Turbulence Summer School, Stanford University*.

Ibragimov, N. H. 1994/1995 *CRC Handbook of Lie Group Analysis of Differential Equations*, Vols 1–3. CRC Press.

Ibragimov, N. H. & Ünal, G. 1994 Lie groups in turbulence. *Lie Groups Applics* **1**(2), 98–103.

Johnston, J. P., Halleen, R. M. & Lazius, D. K. 1972 Effects of spanwise rotation on the structure of two-dimensional fully developed turbulent channel flow. *J. Fluid Mech.* **56**, 533–557.

Kármán, Th. von 1930 Mechanische Ähnlichkeit und Turbulenz. *Nachr. Ges. Wiss. Göttingen* **68**.

Khor'kova, N. G. & Verbovetsky, A. M. 1995 On symmetry subalgebras and conservation laws of the k–ε turbulence model and the Navier–Stokes equations. *Am. Math. Soc. Trans.* **167**(2), 61–90.

Kim, J., Moin, P. & Moser, R. 1987 Turbulence statistics in fully developed channel flow at low Reynolds number. *J. Fluid Mech.* **177**, 133–166.

Kristoffersen, R. & Andersson, H. I. 1993 Direct simulations of low-Reynolds-number turbulent flow in a rotating channel. *J. Fluid Mech.* **256**, 163–197.

Lee, M. J. & Kim, J. 1991 The structure of turbulence in a simulated plane Couette flow. *8th Symp. on Turbulent Shear Flows, Munich, Paper 5-3.*

MACSYMA 1996 *Mathematics and System Reference Manual*, 16th Edn. Macsyma Inc.

Mellor, G. L. 1972 The large Reynolds number asymptotic theory of turbulent boundary layers. *Intl J. Engng Sci.* **10**, 851–873.

Millikan, C. B. 1939 A critical discussion of turbulent flows in channels and circular tubes. *Proc. 5th Intl Congr. Appl. Mech.* Cambridge.

Niederschulte, G. L. 1996 Turbulent flow through a rectangular channel. PhD thesis, University of Illinois, Department of Theoretical and Applied Mechanics.

Ning, L., Hu, Y., Ecke, R. E., Ahlers, G. 1993 Spatial and temporal averages in chaotic patterns. *Phys. Rev. Lett.* **71**, 2216–2219.

Oberlack, M. 1995 Analysis of the two-point velocity correlations in turbulent boundary layer flows. *Center for Turbulence Research, NASA Ames/Stanford University, Annual Research Briefs 1995.*

Oberlack, M. 1999 Similarity in non-rotating and rotating turbulent pipe flows. *J. Fluid Mech.* **379**, 1–22.

Roth, R. 1970 On the existence of a relation between the Kolmogoroff and the von Kármán constants. *Boundary-Layer Metr.* **1**, 131–136.

Saddoughi, S. G. & Veeravalli, S. V. 1994 Local isotropy in turbulent boundary layers at high Reynolds number. *J. Fluid Mech.* **268**, 333–372.

Schlichting, H. 1979 *Boundary-Layer Theory*. McGraw-Hill.

Stephani, H. 1989 *Differential Equations: Their Solution Using Symmetries*. Cambridge University Press.

Townsend, A. A. 1976 *Structure of Turbulent Shear Flow*. Cambridge University Press.

Ünal, G. 1994 Application of equivalence transformations to inertial subrange of turbulence. *Lie Groups Applics* **1**(1), 232–240.

Ünal, G. 1995 Equivalence transformations of the Navier–Stokes equations and the inertial range of turbulence. *Proc. 8th Intl Symp. on Continuum Models and Discrete Systems* (ed. K. Z. Markov), pp. 480–487. World Scientific.

Wei, T. & Willmarth, W. W. 1989 Reynolds-number effects on the structure of a turbulent channel flow. *J. Fluid Mech.* **204**, 57–95.

Yajnik, K. S. 1970 Asymptotic theory of turbulent shear flows. *J. Fluid Mech.* **42**, 411–427.

Zagarola, M. V. 1996 Mean-flow scaling of turbulent pipe flow. Dissertation, Princeton University.